

# Pion-production cross sections in neutrino reactions for studying generalized parton distributions of the nucleon

Xurong Chen,<sup>1,2,3</sup> S. Kumano,<sup>4,5,1</sup> R. Kunitomo,<sup>4</sup> Siyu Wu,<sup>1,3</sup> and Ya-Ping Xie<sup>1,2</sup>

<sup>1</sup>*Institute of Modern Physics, Chinese Academy of Sciences, Lanzhou 730000, China*

<sup>2</sup>*University of Chinese Academy of Sciences, Beijing 100049, China*

<sup>3</sup>*South China Normal University, Guangzhou 510006, China*

<sup>4</sup>*Department of Mathematics, Physics, and Computer Science, Faculty of Science, Japan Women's University, Mejirodai 2-8-1, Bunkyo-ku, Tokyo 112-8681, Japan*

<sup>5</sup>*KEK Theory Center, Institute of Particle and Nuclear Studies, KEK, Oho 1-1, Tsukuba, Ibaraki, 305-0801, Japan*

Spacelike and timelike generalized parton distributions (GPDs) have been investigated at charged-lepton accelerator facilities, for example, by the virtual Compton scattering and the two-photon process, respectively. In this work, we show the  $\pi^\pm$  and  $\pi^0$  production cross sections in neutrino (antineutrino) reactions  $\nu(\bar{\nu}) + N \rightarrow \ell + \pi + N'$  for studying the GPDs of the nucleon by using the theoretical formalism of Pire, Szymanowski, and Wagner. The  $\pi^\pm$ -production cross sections are useful for finding mainly gluon GPDs, whereas the  $\pi^0$  production probes quark GPDs, although there are sizable quark-gluon interference terms in the  $\pi^\pm$  production. In particular, we show the roles of the pion- and rho-pole terms, the contribution from each GPD term ( $H$ ,  $E$ ,  $\tilde{H}$ ,  $\tilde{E}$ ), the effects of the gluon GPDs  $H_g$  and  $E_g$ , and the dependence on the energy of the process in the neutrino cross sections. These cross sections could be measured at Fermilab in future. The neutrino GPD studies will play a complementary role to the projects of charged-lepton and hadron reactions for determining the accurate GPDs.

## I. INTRODUCTION

Understanding the origin of masses in nature is one of important issues as fundamental physics. The origin of hadron masses is not easily understood because the hadrons are many-body systems of quarks and gluons, and the masses are created by complicated emergent mechanisms of their elementary constituents. The mass distributions in hadrons are investigated by gravitational form factors (GFFs), which provide key information for understanding the origin of the hadron masses. Because the gravitational interactions are too weak to measure the GFFs, in comparison with the strong, electromagnetic, and weak interactions, the GFFs used to be considered purely academic quantities without any experimental measurement until several years ago.

The situation has changed because of the development of hadron-tomography field in terms of generalized parton distributions (GPDs) [1–3]. The second moments of the GPDs are related to the form factors of the energy-momentum tensor of quarks and gluon. These form factors are conventionally called the GFFs because a graviton couples to a quark or a gluon in the form of the energy-momentum tensor. Alternatively, they are simply called the form factors of the energy-momentum tensor. Therefore, without relying on the direct gravitational interactions, one can measure the GFFs through the electromagnetic interactions, or weak interactions as shown in this paper. In fact, gravitational radii were determined for the pion by using the two-photon experimental data of the KEK-B factory [4, 5]. The two-photon process or the  $s$ -channel Compton scattering is also possible by using the ultraperipheral hadron collisions [6]. Furthermore, the gravitational form factor and

mass radius were also determined for the proton by using the vector-meson photo-production data [7]. On the other hand, the renormalization of the quark and gluon energy-momentum tensors was investigated in perturbative quantum chromodynamics (QCD) [8]. The GPDs also contain pressure and shear force information in the hadrons [5, 9], so their kinematical stability should be clarified.

The GPDs will provide not only the gravitational information, such as the mass and pressure distributions, but also information on solving the origin of hadron spins by clarifying orbital angular momentum contributions [1, 3]. The GPDs contain three dimensional quark and gluon distributions, namely longitudinal parton distribution functions (PDFs) and transverse form factors in the hadrons. Because of this nature, the GPDs could be used also for clarifying structure of exotic hadron candidates in future [10].

The spacelike GPDs have been investigated by the deeply virtual Compton scattering (DVCS) ( $\gamma^* + h \rightarrow \gamma + h$ ) where  $\gamma$  is a photon and  $h$  is a hadron, meson ( $M$ ) productions ( $\gamma^* + h \rightarrow M + h$ ), and  $J/\psi$  production ( $\gamma^* + h \rightarrow J/\psi + h$ ) [7]. The generalized distribution amplitudes (GDAs) were studied by the two-photon processes or  $s$ -channel Compton scattering ( $\gamma^* + \gamma \rightarrow h + \bar{h}$ ) [4, 5]. The GDAs could be called the  $s$ -channel GPDs because they are investigated by the  $s$ - $t$  crossing process of the virtual Compton scattering, where  $s$  and  $t$  are Mandelstam variables, and because the GDAs contain timelike form factors. In addition, the GPDs could be investigated in hadron reactions such as the exclusive Drell-Yan ( $\pi + N \rightarrow \mu^+ \mu^- + B$ ) [11] and the hadronic  $2 \rightarrow 3$  processes ( $N + N \rightarrow N + \pi + B$ ) [12–14] where  $B$  is a baryon. There is also a recent theoretical proposal to in-

investigate the GPDs by the  $2 \rightarrow 3$  reactions  $\pi N \rightarrow \gamma\gamma N$ ,  $hM_A \rightarrow h\gamma M_B$ , and  $hM_A \rightarrow hM_B M_C$  where  $M_{A,B,C}$  are mesons [15]. Furthermore, pseudoscalar-meson production processes could be studied for determining the GPDs at future electron-ion colliders (EICs) [16]. The GPDs could be also investigated for hadrons with higher spins, such as spin 1 like the deuteron [17] and spin 3/2 like  $\Delta$  and  $\Omega$  [18].

In this work, we show that the GPDs can be studied in weak-interaction processes by showing neutrino cross sections and their relations to the GPDs. Neutrino reactions are complementary to charged-lepton deep inelastic scattering experiments in determining structure functions and parton distribution functions (PDFs) of the nucleon. The neutrino reactions are sensitive to the quark flavor (*e.g.*  $d + W^+ \rightarrow u$ ,  $s + W^+ \rightarrow c$ ), whereas the charged-lepton cross sections are proportional to quark-charge squared  $e_q^2$ . In addition, the valence-quark distributions are determined by the structure function  $F_3$ , and the strange-quark distribution is found by the neutrino-induced opposite-sign dimuon production.

So far, there is no experimental project on the GPDs in neutrino reactions. However, as obvious in the unpolarized PDF determination, the neutrino reactions should be valuable also in the GPD studies. Fortunately, the high-energy neutrino and antineutrino beams will become available at the Long-Baseline Neutrino Facility (LBNF) of Fermilab in the energy region of 2-15 GeV [19, 20], and it can be used for the GPD and GFF studies. In addition, there is a possibility that the neutrinos from stored muons (nuSTORM) projects [21, 22] could have high-energy neutrino beam option for the GPD studies.

Theoretically, there were following cross section estimates for studying the GPDs in the neutrino reactions. In Ref. [23],  $D_s$  production in neutrino scattering was investigated. Deeply virtual neutrino scattering (DVNS) was formulated for the neutral current [24] and the charged current [25]. A detailed comprehensive analysis was given for the DVNS process for the charge and neutral current amplitudes and cross sections at the leading twist [26]. Neutrino-induced pion production process was investigated in Ref. [27] as an extension of the pion electroproduction. The  $\pi$ ,  $K$ , and  $\eta$  productions in neutrino scattering were studied at the leading twist and the leading order [28]. Twist-3 contributions to the pion production were investigated with the chiral-odd transversity GPDs [29]. By the  $D$ -meson production, the transversity chiral-odd GPDs could be found by the cross sections up to  $m_c/Q$  [30]. NLO corrections to the pion and kaon productions were investigated in Ref. [31]. The pseudoscalar charmed-meson production was studied in the leading order by including the gluon GPDs [32], whereas previous studies were only on the quark GPDs. The most updated information was given in the formalism of Pire, Szymanowski, and Wagner in 2017 (PSW-2017) [33] for productions of light mesons by including gluon GPD contributions.

We calculate the neutrino cross sections by using the

formalism of the PSW-2017 and try to show

1. contribution from each GPD ( $H$ ,  $E$ ,  $\tilde{H}$ ,  $\tilde{E}$ ),
2. effects of pion- and rho-meson pole GPDs,
3. effects of the gluon GPDs  $H_g$  and  $E_g$ ,
4. dependence on the energy of the process,

in the cross sections. The meson-pole terms exist in the Efremov-Radyushkin-Brodsky-Lepage (ERBL) region, which is not experimentally investigated so far [12–14]. It is valuable to show the effects of these undetermined GPDs in the neutrino and antineutrino cross sections. Because the unpolarized gluon distribution is determined relatively well from various experiments, there are some constraints on the gluon GPD  $H_g$ . However, the gluon GPD  $E_g$  is not determined at this stage. Since the LBNF experiment is under preparation for the GPD experiment, it is valuable to show the reliable cross sections numerically and to clarify what kind of the GPDs can be studied in the neutrino reactions in comparison with the charged-lepton GPD studies at the Thomas Jefferson National Accelerator Facility (JLab), CERN-AMBER, KEK-B and future EICs [34].

This paper consists of the following. In Sec. II, the cross section formalism is shown with a brief introduction to the GPDs and pion- and rho-distribution amplitudes. Cross section results are shown in Sec. III for the  $\pi^+$  and  $\pi^0$  productions in neutrino reactions.

## II. NEUTRINO-NUCLEON CROSS SECTIONS AND GPDs

### A. Generalized parton distributions

The GPDs are investigated in the neutrino reaction  $W^*(q) + N(p) \rightarrow \pi(q') + N(p')$ , and they are expressed by the three variables, the Bjorken variable  $x$ , the skewness parameter  $\xi$ , and the momentum-transfer squared  $t$ . These variables are expressed by the initial (final) nucleon,  $W$ , and pion momenta  $p$  ( $p'$ ),  $q$ , and  $q'$ , respectively. The average momenta  $\bar{P}$  and  $\bar{q}$  and the momentum transfer  $\Delta$  are defined by

$$\bar{P} = (p + p')/2, \quad \bar{q} = (q + q')/2, \quad \Delta = p' - p = q - q'. \quad (1)$$

Then,  $Q^2$ ,  $\bar{Q}^2$  and the GPD variables  $x$ ,  $\xi$ , and  $t$  are expressed as

$$Q^2 = -q^2, \quad \bar{Q}^2 = -\bar{q}^2, \\ x = \frac{Q^2}{2p \cdot q}, \quad \xi = \frac{\bar{Q}^2}{2\bar{P} \cdot \bar{q}}, \quad t = \Delta^2. \quad (2)$$

For the reaction with  $Q^2 \gg |t|$ , the skewness parameter is directly related to the variable  $x$  as [10]

$$\xi = \frac{x[1 + t/(2Q^2)]}{2 - x(1 - t/Q^2)} \simeq \frac{x}{2 - x} \quad \text{for } Q^2 \gg |t|. \quad (3)$$

Because this relation is generally satisfied in considered neutrino reactions of this work, it is used in our numerical analysis.

These quantities are expressed by the lightcone variables  $a = (a^+, a^-, \vec{a}_\perp)$ . The variables  $a^\pm$  are defined by  $a^\pm = (a^0 \pm a^3)/\sqrt{2}$ , and  $\vec{a}_\perp$  is the transverse vector. By neglecting the nucleon mass, the nucleon and photon momenta are expressed as

$$\begin{aligned} p &\simeq (p^+, 0, \vec{0}_\perp), & p' &\simeq (p'^+, 0, \vec{0}_\perp), \\ q &\simeq \left(-xp^+, \frac{Q^2}{2xp^+}, \vec{0}_\perp\right), & q' &\simeq \left(0, \frac{Q^2}{2xp^+}, \vec{0}_\perp\right), \end{aligned} \quad (4)$$

where the relation  $(p^+)^2, Q^2 \gg m_N^2, |t|$  is assumed, and the momentum conservation indicates  $p'^+ \simeq (1-x)p^+$ . Here,  $m_N$  is the nucleon mass. Then, the variable  $x$  and  $\xi$  are written by the lightcone variables as

$$x \simeq \frac{k^+}{P^+}, \quad \xi \simeq -\frac{\Delta^+}{P^+}, \quad (5)$$

with the total momentum  $P = p+p'$  and the average parton momentum  $k$  between the initial and final partons, as shown in Fig. 1, in the nucleon. The scaling variable  $x$  is the momentum fraction carried by a parton, and the skewness parameter  $\xi$  is the momentum-transfer fraction from the initial nucleon to the final nucleon or from the initial quark to the final quark.

There are three kinematical regions in the GPDs depending on the scaling variable  $x$  and a skewness parameter  $\xi$ :

- (a)  $-1 < x < -\xi$ : antiquark distribution,
- (b)  $-\xi < x < \xi$ : meson (quark-antiquark) distribution,
- (c)  $\xi < x < 1$ : quark distribution.

The regions (a) and (c) are called the Dokshitzer-Gribov-Lipatov-Altarelli-Parisi (DGLAP) regions, and the region (b) is called the ERBL region. All of these regions need to be understood for clarifying the GPD functions.

The GPDs are defined by the off-forward matrix element of bilocal quark (and gluon) operators with a light-like separation as

$$\begin{aligned} &\int \frac{dy^-}{4\pi} e^{ixP^+y^-} \langle p' | \bar{q}(-y/2) \gamma^+ q(y/2) | p \rangle_{y^+ = \bar{y}_\perp = 0} \\ &= \frac{1}{2P^+} \bar{u}(p') \left[ H^q(x, \xi, t) \gamma^+ + E^q(x, \xi, t) \frac{i\sigma^{+\alpha} \Delta_\alpha}{2m_N} \right] u(p), \end{aligned} \quad (6)$$

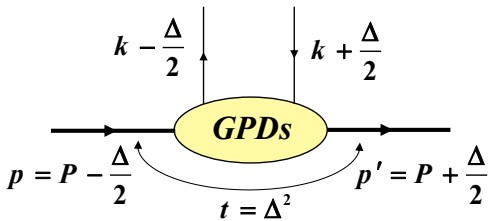


FIG. 1. GPD kinematics.

$$\begin{aligned} &\int \frac{dy^-}{4\pi} e^{ixP^+y^-} \langle p' | \bar{q}(-y/2) \gamma^+ \gamma_5 q(y/2) | p \rangle_{y^+ = \bar{y}_\perp = 0} \\ &= \frac{1}{2P^+} \bar{u}(p') \left[ \tilde{H}^q(x, \xi, t) \gamma^+ \gamma_5 + \tilde{E}^q(x, \xi, t) \frac{\gamma_5 \Delta^+}{2m_N} \right] u(p), \end{aligned} \quad (7)$$

where  $u(p)$  denote the Dirac spinor for the nucleon, and  $\sigma^{\alpha\beta}$  is defined by  $\sigma^{\alpha\beta} = (i/2)[\gamma^\alpha, \gamma^\beta]$ . In these equations, we abbreviated the gauge-link operator between the two quark fields for the color gauge invariance. The functions  $H^q(x, \xi, t)$  and  $E^q(x, \xi, t)$  are the unpolarized quark GPDs, and  $\tilde{H}^q(x, \xi, t)$  and  $\tilde{E}^q(x, \xi, t)$  are the polarized ones. We also do not write the scale dependence of the GPDs from that of the bilocal operators explicitly.

Three important features of the GPDs are the following. First, the functions  $H^q(x, \xi, t)$  and  $\tilde{H}^q(x, \xi, t)$  become the unpolarized and longitudinally-polarized PDFs in the forward limit

$$H^q(x, 0, 0) = q(x), \quad \tilde{H}^q(x, 0, 0) = \Delta q(x). \quad (8)$$

Second, the first moments of  $H^q(x, \xi, t)$ ,  $E^q(x, \xi, t)$ ,  $\tilde{H}^q(x, \xi, t)$ , and  $\tilde{E}^q(x, \xi, t)$  are the Dirac, Pauli, axial and pseudoscalar form factors, respectively

$$\begin{aligned} &\int_{-1}^1 dx H^q(x, \xi, t) = F_1^q(t), \quad \int_{-1}^1 dx E^q(x, \xi, t) = F_2^q(t), \\ &\int_{-1}^1 dx \tilde{H}^q(x, \xi, t) = g_A^q(t), \quad \int_{-1}^1 dx \tilde{E}^q(x, \xi, t) = g_P^q(t). \end{aligned} \quad (9)$$

Third, the second moments of  $H^q(x, \xi, t = 0) + E^q(x, \xi, t = 0)$  indicate the contributions from the quark angular momenta

$$\begin{aligned} J^q &= \frac{1}{2} \int_{-1}^1 dx x [H^q(x, \xi, t = 0) + E^q(x, \xi, t = 0)] \\ &= \frac{1}{2} \Delta q + L^q, \end{aligned} \quad (10)$$

so that the quark orbital-angular-momentum contribution  $\sum_q L^q$  should become clear to the nucleon spin.

The nucleon mass is defined by the matrix element [3]

$$m_N = \left\langle N(p) \left| \int d^3r T^{00}(\vec{r}) \right| N(p) \right\rangle, \quad (11)$$

where the static energy-momentum tensor  $T^{\mu\nu}(\vec{r})$  is defined in the Breit frame as

$$T^{\mu\nu}(\vec{r}) = \int \frac{d^3q}{(2\pi)^3 2E} e^{i\vec{q}\cdot\vec{r}} \langle N(p') | T^{\mu\nu}(0) | N(p) \rangle, \quad (12)$$

with  $E = \sqrt{m_N^2 + \vec{q}^2/4}$ , and the energy-momentum tensor  $T^{\mu\nu}$  on the right-hand side is given by the quark and gluon fields as

$$\begin{aligned} T^{\mu\nu}(x) &= \bar{q}(x) \gamma^{(\mu} i \overleftrightarrow{D}^{\nu)} q(x) \\ &\quad + \left[ \frac{1}{4} g^{\mu\nu} F^2(x) - F^{\mu\alpha}(x) F_\alpha^\nu(x) \right] \\ &\equiv T_q^{\mu\nu}(x) + T_g^{\mu\nu}(x). \end{aligned} \quad (13)$$

Here,  $D$  is the covariant derivative defined by  $D_\mu = \partial_\mu - igT^a A_\mu^a(x)$  with the QCD coupling constant  $g$  and the gluon field  $A_\mu = \sum_{a=1}^{N^2-1} T^a A_\mu^a$  ( $\equiv T^a A_\mu^a$ ) where  $T^a$  is expressed by the Gell-Mann matrix  $\lambda^a$  as  $T^a = \lambda^a/2$ . The derivative  $\overleftrightarrow{D}$  is  $f_1 \overleftrightarrow{D} f_2 = f_1(Df_2) - (Df_1)f_2$ . The first term of the right-hand side in Eq. (13) is symmetrized under the indices as  $A^{(\mu B^\nu)} = (A^\mu B^\nu + A^\nu B^\mu)/2$ . The gluon field strength  $F_{\mu\nu}^a(x)$  is  $F_{\mu\nu}^a(x) = \partial_\mu A_\nu^a(x) - \partial_\nu A_\mu^a(x) + g f^{abc} A_\mu^b(x) A_\nu^c(x)$ , where  $f^{abc}$  the structure constant of the  $SU(3)$  group. In Eq. (13), the gluon field strength  $F$  is  $F^{\mu\nu} = F_a^{\mu\nu} T_a$ , and  $F^2$  is  $F^2 = F^{\mu\nu} F_{\mu\nu}$ .

We write the matrix element of the energy-momentum tensor in terms of the gravitational form factors  $A$ ,  $B$ ,  $C$ , and  $D$  of the nucleon as [9]

$$\begin{aligned} \langle N(p') | T_{q,g}^{\mu\nu}(0) | N(p) \rangle &= \bar{u}(p') \left[ A_{q,g} \gamma^{(\mu} \bar{P}^{\nu)} \right. \\ &+ B_{q,g} \frac{\bar{P}^{(\mu} \sigma^{\nu)\alpha} \Delta_\alpha}{2m_N} + D_{q,g} \frac{\Delta^\mu \Delta^\nu - g^{\mu\nu} \Delta^2}{m_N} \\ &\left. + \bar{C}_{q,g} m_N g^{\mu\nu} \right] u(p). \end{aligned} \quad (14)$$

The form factor  $A$  indicates the mass (energy) distribution,  $B$  does the angular momentum distribution,  $D$  does the pressure distribution, and  $\bar{C}$  does the mass and pressure distribution. Its  $\mu\nu = 00$  component corresponds to the mass distribution in the nucleon:

$$\begin{aligned} \langle N(p') | T_{q,g}^{00}(0) | N(p) \rangle &= 2m_N E \left[ A_{q,g}(t) \right. \\ &\left. - \frac{t}{4m_N^2} \{ A_{q,g}(t) - 2B_{q,g}(t) + D_{q,g}(t) \} + \bar{C}_{q,g}(t) \right]. \end{aligned} \quad (15)$$

These gravitational form factors are expressed by the GPDs as

$$\begin{aligned} \int_{-1}^1 dx x H^{q,g}(x, \xi, t) &= A_{q,g}(t) + 4\xi^2 D_{q,g}(t), \\ \int_{-1}^1 dx x E^{q,g}(x, \xi, t) &= B_{q,g}(t) - 4\xi^2 D_{q,g}(t). \end{aligned} \quad (16)$$

If these GPDs of the nucleon are determined, it leads to the understanding to the origin of the nucleon mass in terms of quarks and gluons.

## B. Pion and rho distribution amplitudes and their-pole GPDs

For describing the pion-production cross section, the pion distribution amplitude is necessary. In addition, we investigate effects of pion- and rho-pole terms in the nucleon GPDs on the cross sections. In these pole terms, the pion- and rho-distribution amplitudes exist. Therefore, their distribution amplitudes and pole GPDs are explained in this subsection.

The twist-2 pion distribution amplitude  $\Phi_\pi(x, \mu)$  is defined by the matrix element between the vacuum and pion states as [11, 35, 36]

$$\begin{aligned} \langle 0 | \bar{d}(0)_\alpha u(y)_\beta | \pi^+(p_\pi) \rangle \Big|_{y^- = \bar{y}_\perp = 0} \\ = \frac{if_\pi}{4} \int_0^1 dx e^{-ixp_\pi^- y^+} (\gamma_5 \not{p}_\pi)_{\beta\alpha} \Phi_\pi(x, \mu), \end{aligned} \quad (17)$$

where higher-twist terms are abbreviated on the right-hand side. The variable  $x$  indicates the momentum fraction of a valence quark in the pion, and  $\mu$  is the renormalization scale of the bilocal operator on the left-hand side of Eq. (17). The pion decay constant  $f_\pi$  is define by  $\langle 0 | \bar{d}(0) \gamma^\mu \gamma_5 u(0) | \pi^+(p_\pi) \rangle = if_\pi p_\pi^\mu$ , and the pion distribution amplitude  $\Phi_\pi(x, \mu)$  satisfies the normalization  $\int_0^1 dx \Phi_\pi(x, \mu) = 1$ .

The pion distribution amplitude is often used in the kinematical region  $0 < x < 1$ . However, the range of the variable  $x$  is between  $-1$  and  $1$  in the GPDs as explained in the previous subsection. The pion distribution amplitude needs to be converted by using this variable. In order to avoid confusion, we express this variable between  $-1$  and  $1$  as  $z$  only in this subsection. Using the relation  $z = 2x - 1$ , we rewrite Eq.(17) as

$$\begin{aligned} \langle 0 | \bar{d}(-y)_\alpha u(y)_\beta | \pi^+(p_\pi) \rangle \Big|_{y^- = \bar{y}_\perp = 0} \\ = \frac{if_\pi}{4} \int_{-1}^1 dz e^{-izp_\pi^- y^+} (\gamma_5 \not{p}_\pi)_{\beta\alpha} \phi_\pi(z, \mu), \end{aligned} \quad (18)$$

where the pion distribution amplitude  $\phi_\pi(z, \mu)$  is expressed by  $\Phi_\pi(x, \mu)$  as

$$\begin{aligned} \phi_\pi(z, \mu) &= \frac{1}{2} \Phi_\pi \left( x = \frac{z+1}{2}, \mu \right), \\ \phi_\pi(z, \mu) &: \quad -1 < z < 1, \\ \Phi_\pi(x, \mu) &: \quad 0 < x < 1, \end{aligned} \quad (19)$$

with the normalization  $\int_{-1}^1 dz \phi_\pi(z, \mu) = 1$ . This relation (19) should be noted in discussing the pion- and rho-pole terms in the GPDs.

The pion state is written by the Fock states in the lightcone quantization as

$$|\pi(p_\pi)\rangle = \int \frac{dx d^2 \vec{k}_T}{16\pi^3 \sqrt{x\bar{x}}} \Psi_{q\bar{q}/\pi}(x, \vec{k}_T) |q(k_q) \bar{q}(k_{\bar{q}})\rangle + \dots, \quad (20)$$

where  $\Psi_{q\bar{q}/\pi}(x, \vec{k}_T)$  is the Bethe-Salpeter (BS) wave function,  $|q(k_q) \bar{q}(k_{\bar{q}})\rangle$  is the  $q\bar{q}$  Fock state, and the ellipsis ( $\dots$ ) indicates higher Fock states. The variables  $x$  and  $\bar{x}(=1-x)$  are momentum fractions of the quark and antiquark, respectively, and  $\vec{k}_T$  is the quark transverse momentum ( $\vec{k}_T \equiv \vec{k}_{qT} = -\vec{k}_{\bar{q}T}$ ). The pion distribution amplitude is given by this BS wave function as [35]

$$\Phi_\pi(x, \mu) = \frac{2\sqrt{2N_c}}{if_\pi} \int_{|\vec{k}_T| < \mu} \frac{d^2 \vec{k}_T}{16\pi^3} \Psi_{u\bar{d}/\pi}(x, \vec{k}_T), \quad (21)$$

with the number of colors  $N_c$ .

In general, the distribution amplitude is expressed by the Gegenbauer polynomials  $C_n^{3/2}$  at  $\mu$  as

$$\Phi_\pi(x, \mu) = 6x(1-x) \sum_{n=0,2,4,\dots}^{\infty} a_n(\mu) C_n^{3/2}(2x-1). \quad (22)$$

In the asymptotic limit  $\mu \rightarrow \infty$  (as), it becomes [37]

$$\Phi_\pi^{\text{as}}(x) = 6x(1-x), \quad (23)$$

whereas the following form with  $a_2(\mu \simeq 0.5 \text{ GeV}) = 2/3$  was proposed by Chernyak and Zhitnitsky (CZ) [36]

$$\Phi_\pi^{\text{CZ}}(x, \mu \simeq 0.5 \text{ GeV}) = 30x(1-x)(2x-1)^2. \quad (24)$$

For calculating the neutrino cross section in Sec. III, the pion distribution amplitude of Ref. [38] is used with  $a_2 = 0.22$  and  $a_{4,6,\dots} = 0$  in Eq. (22). The rho distribution amplitude  $\Phi_\rho(x, \mu)$  is also given in the same way [39], and its asymptotic form is given as

$$\Phi_\rho^{\text{as}}(x) = 6x(1-x). \quad (25)$$

Using these distribution amplitudes, we write the pion- and rho-pole contributions to the GPDs. The pion- and rho-pole GPDs are given in Ref. [12], and different normalizations are used for their distribution amplitudes from the ones explained in this section. The pion decay constant, pion distribution amplitude, and rho distribution amplitude of Ref. [12] are denoted  $f'_\pi$ ,  $\Phi'_\pi$ , and  $\Phi'_\rho$  to avoid confusion. Then, they are related to  $f_\pi$ ,  $\Phi_\pi$ , and  $\Phi_\rho$  in this section as

$$f'_\pi = \frac{1}{\sqrt{2}} f_\pi, \quad \Phi'_\pi(x) = \frac{f_\pi}{2\sqrt{6}} \Phi_\pi(x), \quad \Phi'_\rho(x) = \frac{f_\rho}{\sqrt{6}} \Phi_\rho(x), \quad (26)$$

with the rho decay constant  $f_\rho$ , so that the Goldberger-Treiman relation is given as  $f'_\pi g_{\pi NN} = m_N g_A$  with the pion-nucleon coupling constant  $g_{\pi NN}$  and the axial charge of the nucleon  $g_A$ .

The pion is a pseudo-scalar hadron and it contributes to the axial GPD  $\tilde{E}(z, \xi, t)$ , where  $z$  is used for indicating the range  $-1 < z < 1$  explicitly in this subsection, as [12, 40, 41]

$$\begin{aligned} \tilde{E}_\pi(z, \xi, t) &= \frac{4g_A m_N^2}{1-t/m_\pi^2} \frac{\sqrt{3}}{m_\pi^2 f'_\pi \xi} \Phi'_\pi \left( x = \frac{z+\xi}{2\xi} \right) \theta(\xi - |z|) \\ &= -m_N f_\pi \frac{2\sqrt{2}g_{\pi NN}}{t-m_\pi^2} \frac{1}{2\xi} \Phi_\pi \left( x = \frac{z+\xi}{2\xi} \right) \theta(\xi - |z|). \end{aligned} \quad (27)$$

The function  $\tilde{E}_\pi$  indicates the isovector combination in terms of up and down quark GPDs as  $(\tilde{E}^u - \tilde{E}^d)_\pi$ . Therefore, each quark GPD is expressed as

$$\tilde{E}^u(z, \xi, t) = -\tilde{E}^d(z, \xi, t) = \frac{1}{2} \tilde{E}_\pi(z, \xi, t). \quad (28)$$

There is no contribution to the GPD  $\tilde{H}$  from the pion.

The rho is a vector hadron, and it contributes to the vector part. The rho-pole GPDs are given by [12, 42]

$$\begin{aligned} H_\rho(z, \xi, t) &= \frac{1}{1-t/m_\rho^2} \frac{C_1}{g_\rho} \frac{1}{2\xi} \Phi_\rho \left( x = \frac{z+\xi}{2\xi} \right) \theta(\xi - |z|), \\ E_\rho(z, \xi, t) &= \frac{1}{1-t/m_\rho^2} \frac{C_2}{g_\rho} \frac{1}{2\xi} \Phi_\rho \left( x = \frac{z+\xi}{2\xi} \right) \theta(\xi - |z|), \end{aligned} \quad (29)$$

where  $g_\rho$  is the vector coupling constant of the rho, and  $m_\rho$  is the rho mass. The  $C_1$  and  $C_2$  are isovector rho coupling constants with the nucleon, and they are given by

$$\frac{C_1}{g_\rho} = \frac{e_p - e_n}{2}, \quad \frac{C_2}{g_\rho} = \frac{\kappa_p - \kappa_n}{2} \quad (30)$$

with the charge of the proton (neutron)  $e_p$  ( $e_n$ ), and  $\kappa_p$  ( $\kappa_n$ ) is the anomalous magnetic moment of the proton (neutron). Then, the quark GPDs are given as

$$\begin{aligned} H^u(z, \xi, t) &= -H^d(z, \xi, t) = \frac{1}{2} H_\rho(z, \xi, t), \\ E^u(z, \xi, t) &= -E^d(z, \xi, t) = \frac{1}{2} E_\rho(z, \xi, t). \end{aligned} \quad (31)$$

These meson contributions to the GPDs exist in the ERLB region and they should be included within the nucleonic GPDs.

### C. Cross section for the pion production in neutrino reactions

As the most recent theoretical formalism for describing the neutrino-induced pion production ( $\nu N \rightarrow \ell N' \pi$ ) cross section by using the GPDs, we use the PSW-2017 [33]. It includes not only quark contributions but also gluon ones for the  $\pi^\pm$  and  $\pi^0$  productions. Since it is a weak-interaction process, it is appropriate to rely on larger cross sections with the pion production experimentally, instead of the photon production in the DVCS.

The pion-production process  $\nu N \rightarrow \ell N' \pi$  is shown in Fig. 2, where  $k$  ( $k'$ ),  $p$  ( $p'$ ),  $q$ , and  $p_\pi$  are the momenta for the initial neutrino (final lepton), the initial (final) nucleon, the W boson, and the pion, respectively. This pion-production cross section is described in a factorized form with the GPDs as typically shown in Fig. 3, where the quark and gluon GPDs contribute to the pion production. In describing its cross section, the kinematical variables  $Q^2$ ,  $x$ ,  $t$ ,  $\Delta$  are defined in Eqs. (1) and (2). In addition,  $y$  is given by  $y = p \cdot q / p \cdot k$ . The momentum-transfer squared  $Q^2$  is expressed by the center-of-mass-energy squared  $s = (p+k)^2$  as  $Q^2 = xy(s - m_N^2)$ .

In general, both quark and gluon GPDs contribute to the pion-production cross section, and their amplitudes

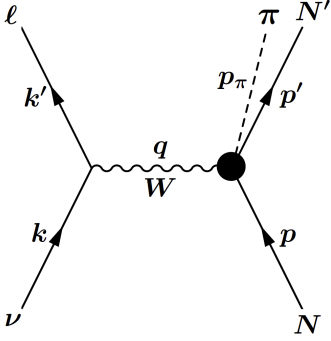


FIG. 2. Pion-production process  $\nu N \rightarrow \ell N' \pi$  in a charged-current neutrino reaction.

$T^q$  and  $T^g$  are given by [33]

$$T^q = -i \frac{C_q}{2Q} \bar{u}(p') \left( \mathcal{H}^q \not{n} - \tilde{\mathcal{H}}^q \not{n} \gamma^5 + \mathcal{E}^q \frac{i\sigma^{n\Delta}}{2m_N} - \tilde{\mathcal{E}}^q \frac{\gamma^5 \Delta \cdot n}{2m_N} \right) u(p),$$

$$T^g = -i \frac{C_g}{2Q} \bar{u}(p') \left( \mathcal{H}^g \not{n} + \mathcal{E}^g \frac{i\sigma^{n\Delta}}{2m_N} \right) u(p). \quad (32)$$

Here, the constants  $C_q$  and  $C_g$  are defined by color and flavor factors as  $C_q = 2\pi C_F \alpha_s V_{du}/3$  with  $C_F = (N_c^2 - 1)/(2N_c) = 4/3$  where the number of color is  $N_c = 3$ , and  $C_g = \pi T_f \alpha_s V_{du}/3$  with  $T_f = 1/2$ . The  $\alpha_s$  is the running coupling constant of QCD, and  $V_{du}$  is the quark mixing angle,  $Q$  is given by  $Q = \sqrt{Q^2}$ ,  $\not{n}$  is given by  $\not{n} \equiv n^\mu \gamma_\mu = \gamma^+$  with  $n^\mu = (1, 0, 0, -1)/\sqrt{2}$ , and  $\sigma^{n\Delta} = \sigma^{\mu\nu} n_\mu \Delta_\nu$ . The functions  $\mathcal{F}^q$  and  $\mathcal{F}^g$  ( $\mathcal{F} = \mathcal{H}, \tilde{\mathcal{H}}, \mathcal{E}, \tilde{\mathcal{E}}$ ) are defined by the integrals as

$$\mathcal{F}^q = 2f_\pi \int_0^1 dx' \frac{\Phi_\pi(x')}{1-x'} \int_{-1}^1 dx \frac{F^q(x, \xi, t)}{x - \xi + i\epsilon},$$

$$\mathcal{F}^g = \frac{8f_\pi}{\xi} \int_0^1 dx' \frac{\Phi_\pi(x')}{x'(1-x')} \int_{-1}^1 dx \frac{F^g(x, \xi, t)}{x - \xi + i\epsilon}, \quad (33)$$

where  $\Phi_\pi(x')$  is the pion distribution amplitude defined in the range  $0 < x' < 1$ , and  $F^q$  and  $F^g$  are quark and gluon GPDs ( $F = H, E, \tilde{H}, \tilde{E}$ ).

The quark GPD contribution is shown on the left-hand side of Fig. 3, where the quark  $q$  could be up, down, strange, or charm quark. In our numerical analyses, the

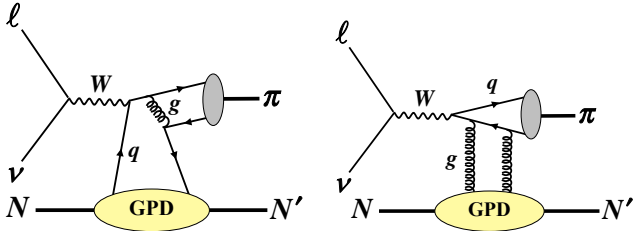


FIG. 3. Typical pion-production processes with quark and gluon GPDs.

strange- and charm-quark contributions are neglected, and the up and down quark GPDs  $F^u$  and  $F^d$  contributions are estimated. If the intermediate W-boson is  $W^+$  ( $\nu p \rightarrow \ell^- W^+ p$ ), a  $d$ -quark is extracted from the proton to interact with  $W^+$  and it becomes a  $u$ -quark to form a  $\pi^+$  together with a  $\bar{d}$  quark. Then, a  $d$ -quark is absorbed into the proton to form a proton in the final state. This amplitude is described by the GPD  $F^d$ . In the same way, the  $W^+$  boson interacts with an anti-quark  $\bar{u}$  in the initial proton. According to Table 1 in the paper of Kopeliovich-Schmidt-Siddikov of 2012 [28], these two process amplitudes are given by  $V_{ud}[H_d(x)c_- + H_u(x)c_+] \rightarrow V_{ud} \int dx [H_d(x)/(x - \xi + i\epsilon) + H_u(x)/(x + \xi - i\epsilon)] = V_{ud} \int dx [H_d(x) - H_u(-x)]/(x - \xi + i\epsilon)$ , where  $c_\pm = 1/(x \pm \xi \mp i\epsilon)$ . Therefore, the charged-current reactions are sensitive to the  $u$ - and  $d$ -quark GPDs by the following combination [33]

$$F^q(x, \xi, t) = F^d(x, \xi, t) - F^u(-x, \xi, t)$$

for the  $\pi^+$  production  $\nu p \rightarrow \ell^- p \pi^+$ . (34)

On the other hand, all the  $u$ ,  $d$ ,  $\bar{u}$ , and  $\bar{d}$  quarks contribute to the  $\pi^0$ -production cross section ( $\bar{\nu} p \rightarrow \ell^+ n \pi^0$ ), and its amplitude is given by  $V_{ud}[H_u(x) - H_d(x)](c_+ - c_-)/\sqrt{2}$  [28]. For the  $\pi^0$  production with the initial neutron ( $\nu n \rightarrow \ell^- p \pi^0$ ), it is given by  $V_{ud}[H_d(x) - H_u(x)](c_+ - c_-)/\sqrt{2}$  by exchanging  $u$  and  $d$  by assuming the isospin symmetry in the GPDs. Therefore, the quark GPD should be written as

$$F^q(x, \xi, t) = \frac{1}{\sqrt{2}} [F^u(x, \xi, t) - F^d(x, \xi, t) + F^u(-x, \xi, t) - F^d(-x, \xi, t)]$$

for the  $\pi^0$  production  $\nu n \rightarrow \ell^- p \pi^0$ . (35)

If the isospin symmetry is valid, both  $\pi^0$  cross sections are equal  $\sigma(\bar{\nu} p \rightarrow \ell^+ n \pi^0) = \sigma(\nu n \rightarrow \ell^- p \pi^0)$ .

In Eq. (33), the integral over  $x$  is given by using the relation with the principal integral and the delta function,  $1/(x - \xi + i\epsilon) = \mathcal{P}/(x - \xi) - i\pi\delta(x - \xi)$ , as

$$\int_{-1}^1 dx \frac{F(x, \xi, t)}{x - \xi + i\epsilon} = \mathcal{P} \int_{-1}^1 dx \frac{F(x, \xi, t)}{x - \xi} - i\pi F(\xi, \xi, t), \quad (36)$$

so that the GPDs in the whole kinematical region of  $x$ , including the ERBL region ( $-\xi < x < \xi$ ), contribute to the cross section. It could mean that the cross section is sensitive to the meson-pole contributions discussed in Sec. II B because the meson-pole GPDs exist in the ERBL region.

Using these quark and gluon amplitudes with the GPDs, we write the neutrino pion-production cross section as [33]

$$\frac{d^4\sigma(\nu N \rightarrow \ell N' \pi)}{dy dQ^2 dt} = 2\pi \bar{\Gamma} \varepsilon \sigma_L. \quad (37)$$

The factor  $\varepsilon$  indicates the fraction of the cross section for the longitudinal photon polarization, and it is defined by

$\varepsilon = 1/[1 - 2\bar{q}^2 \tan^2(\theta/2)/q^2]$ , which is approximated as  $\varepsilon \simeq (1-y)/(1-y+y^2/2)$ , with the scattering angle  $\theta$  for the lepton [43]. The  $\bar{\Gamma}$  is the kinematical factor given by

$$\bar{\Gamma} = \frac{G_F^2 Q^2}{32(2\pi)^4 y \sqrt{1 + 4x_B^2 m_N^2 / Q^2 (s - m_N^2)^2 (1 - \varepsilon)}}, \quad (38)$$

where  $G_F$  is the Fermi coupling constant. The longitudinal cross section  $\sigma_L = \epsilon_L^{*\mu} \epsilon_L^\nu W_{\mu\nu}$  for  $W(\epsilon_L)N \rightarrow \pi N'$  is expressed as

$$\begin{aligned} \sigma_L = \frac{1}{Q^2} \left\{ \right. & \left[ |C_q \mathcal{H}^q + C_g \mathcal{H}^g|^2 + |C_q \tilde{\mathcal{H}}^q|^2 \right] (1 - \xi^2) \\ & + \frac{\xi^4}{1 - \xi^2} \left[ |C_q \mathcal{E}^q + C_g \mathcal{E}^g|^2 + |C_q \tilde{\mathcal{E}}^q|^2 \right] \\ & - 2\xi^2 \text{Re} [(C_q \mathcal{H}^q + C_g \mathcal{H}^g)(C_q \mathcal{E}^q + C_g \mathcal{E}^g)^*] \\ & \left. - 2\xi^2 \text{Re} [(C_q \tilde{\mathcal{H}}^q)(C_q \tilde{\mathcal{E}}^q)^*] \right\}. \quad (39) \end{aligned}$$

Although both  $\mathcal{H}^q$  and  $\mathcal{H}^g$  ( $\mathcal{E}^q$  and  $\mathcal{E}^g$ ) exist in this equation, only the quark terms  $\mathcal{H}^q$  and  $\mathcal{E}^q$  exist without the gluon contributions. As explained in Ref. [33], the gluon axial amplitude vanishes by summing the considered gluon processes, so that there is no  $\mathcal{H}^g$  and  $\mathcal{E}^g$  in the cross section. The functions  $\mathcal{H}^q, \mathcal{H}^g, \dots$ , which are called Compton form factors, will be determined from the cross section in Eq. (39). These Compton form factors are related to the corresponding GPDs by the relations in Eq. (33). In order to obtain the GPDs from the Compton form factors, deconvolution is necessary, and there were recent studies on this issue with a shadow GPD problem [44]. The same deconvolution issue exists in the neutrino reactions. Once the neutrino cross sections are measured in future, one should be careful about handling this problem. In this way, if the neutrino cross sections are measured for the pion production, the GPDs could be determined by a global analysis together with the charged-lepton GPD experiments.

### III. RESULTS

#### A. Used GPDs for calculating cross sections

The GPDs are still not well determined yet from global analysis. There are three variables  $x$ ,  $\xi$ , and  $t$  for describing the GPDs. In the current charged-lepton measurements, the full kinematical region cannot be investigated including the ERBL region  $-\xi < x < \xi$ . Therefore, the current versions of the GPD parametrizations need improvements to become a similar status of the unpolarized-PDF parametrizations. Nonetheless, there are constraints on some GPDs. For understanding them intuitively, let us consider possibly the simplest factorized form, for example, for the GPDs  $H$  at  $\xi = 0$  as [45]

$$H^i(x, \xi = 0, t) = f_i(x) F_i(t, x), \quad i = q, g, \quad (40)$$

where  $f_i(x)$  is a longitudinal PDF,  $F_i(t, x)$  is a transverse form factor at  $x$ , and  $i$  indicates a quark or gluon. Therefore, the  $x$  and  $t$  distributions are constrained by the longitudinal PDFs and the form factors, which can be investigated in other experiments. Especially, the GPDs  $H$  and  $\tilde{H}$  should be constrained by the unpolarized and longitudinally-polarized PDFs, respectively.

As a useful model for the GPDs, we use the Goloskokov-Kroll (GK) parametrization proposed in a series of papers in Refs. [46]. These works were summarized in Ref. [38], so that it is sometimes called the GK-2013 parametrization. It is accommodated as the GK model in the code of the PARTONS project [2] for the GPDs. We use the GK parametrization with modifications for the gluon GPD  $E_g$  and by including the rho-pole effects in the GPDs  $H_q$  and  $E_q$ . On the GPDs  $E$ , their parameters are not shown in Ref. [38], so that the 2009 version of the GK is taken [46]. We use the GPDs  $\tilde{E}_q$  including the pion-pole terms, which exist in the GK parametrization, whereas the rho-pole term does not exist in the GK. These GPD modifications from the original GK parametrization are explained in showing the numerical results in the next subsection.

The general form of the GK parametrization is given in the integral form as [38]

$$\begin{aligned} F^i(x, \xi, t) = \int_{-1}^1 d\rho \int_{-1+|\rho|}^{1-|\rho|} d\eta \delta(\rho + \xi\eta - x) f^i(\rho, \eta, t) \\ + D_i(x, t) \Theta(\xi^2 - x^2), \quad (41) \end{aligned}$$

where  $\Theta(\xi^2 - x^2)$  is the Heaviside step function

$$\Theta(\xi^2 - x^2) = \begin{cases} 1 & (\xi^2 > x^2) \\ 0 & (\xi^2 < x^2) \end{cases}. \quad (42)$$

In the GK-2013, the term  $D_i(x, t) \Theta(\xi^2 - x^2)$  exists only in the GPD  $\tilde{E}$  because the pion-pole GPD is included. In our numerical analysis of this work, we also include rho-pole GPDs  $H$  and  $E$ , so that such D terms exist in these GPDs. The double parton distributions  $f^i$  are parametrized in the following way:

$$f^i(\rho, \eta, t) = F^i(\rho, \xi = 0, t) w_i(\rho, \eta),$$

$$F^i(\rho, \xi = 0, t) = F^i(\rho, \xi = 0, t = 0) \exp(t p_{fi}(\rho)),$$

$$p_{fi}(\rho) = -\alpha'_{fi} \ln \rho + b_{fi},$$

$$w_i(\rho, \eta) = \frac{\Gamma(2n_i + 2)}{2^{2n_i+1} \Gamma^2(n_i + 1)} \frac{[(1 - |\rho|)^2 - \eta^2]^{n_i}}{(1 - |\rho|)^{2n_i+1}}. \quad (43)$$

The parameters were determined from a global analysis. The distributions in the negative  $x$  region should be understood by discussing valence- and sea-quark separately as

$$\begin{aligned} F_{\text{val}}^q(-x, \xi, t) &= 0, & -1 \leq x \leq -\xi, \\ F_{\text{sea}}^q(-x, \xi, t) &= -\epsilon_f F_{\text{sea}}^q(x, \xi, t), \\ F^g(-x, \xi, t) &= \epsilon_f F^g(x, \xi, t), \quad (44) \end{aligned}$$

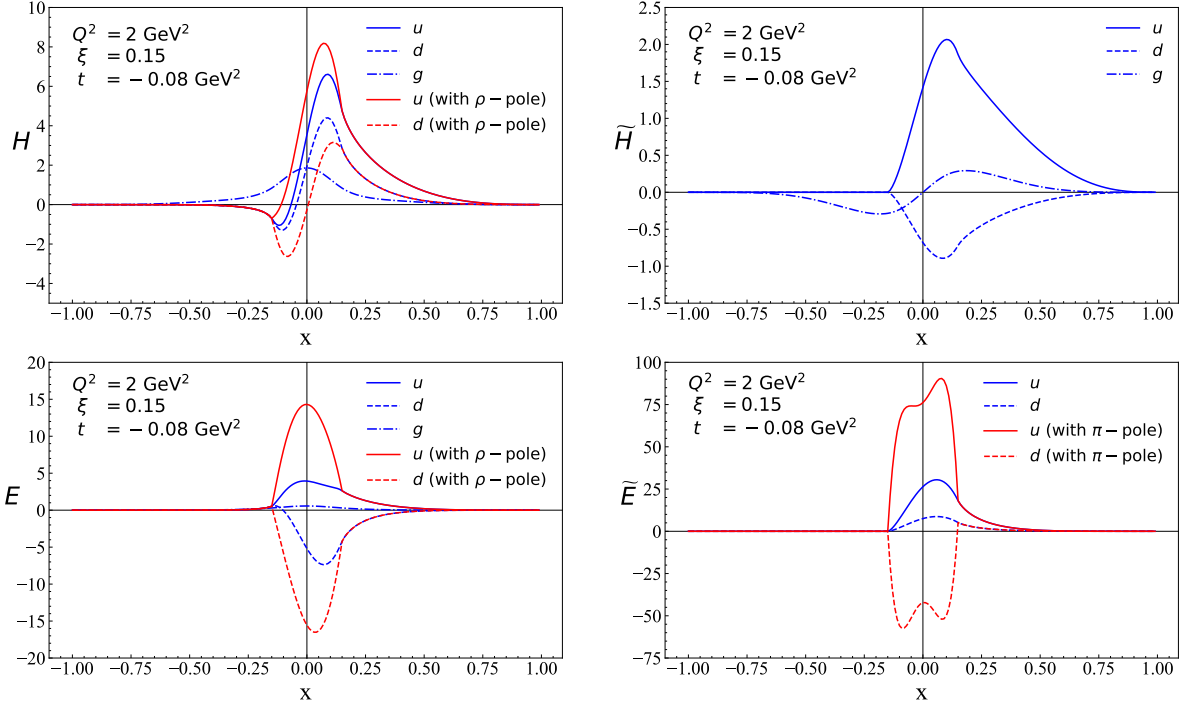


FIG. 4. GPDs of the GK parametrization, with the additional rho-pole terms, are shown as the function of  $x$  at  $Q^2=2 \text{ GeV}^2$ ,  $\xi = 0.15$ ,  $t = -0.08 \text{ GeV}^2$ . The quark GPDs  $H^{u,d}$ ,  $E^{u,d}$ , and  $\tilde{E}^{u,d}$  are shown with and without the pion- and rho-pole GPDs.

where  $\epsilon_f = 1$  for the GPDs  $H$  and  $E$  and  $\epsilon_f = -1$  for the GPDs  $\tilde{H}$  and  $\tilde{E}$ . The parameter values are listed in the tables of Refs. [38, 46]. In the integral of Eq. (41), one needs to be careful about separate treatments on valence-quark, sea-quark, and gluon integrals as

$$\begin{aligned}
 \text{valence: } & \int_0^1 d\rho \int_{-1+|\rho|}^{1-|\rho|} d\eta \delta(\rho + \xi\eta - x) f_{\text{val}}^q(|\rho|, \eta, t), \\
 \text{sea: } & \int_0^1 d\rho \int_{-1+|\rho|}^{1-|\rho|} d\eta \delta(\rho + \xi\eta - x) f_{\text{sea}}^q(|\rho|, \eta, t) \\
 & - \int_{-1}^0 d\rho \int_{-1+|\rho|}^{1-|\rho|} d\eta \delta(\rho + \xi\eta - x) f_{\text{sea}}^q(|\rho|, \eta, t), \\
 \text{gluon: } & \int_{-1}^1 d\rho \int_{-1+|\rho|}^{1-|\rho|} d\eta \delta(\rho + \xi\eta - x) f^g(|\rho|, \eta, t). \quad (45)
 \end{aligned}$$

One can use these functions with the parameter values for numerical evaluations or simply use the PARTONS code for the GK model [2].

The obtained GPDs are shown in Fig. 4 by taking  $Q^2=2 \text{ GeV}^2$ ,  $\xi = 0.15$ ,  $t = -0.08 \text{ GeV}^2$ . The  $u$ -quark,  $d$ -quark, and gluon distributions are shown except for  $\tilde{E}$ , where there is no gluon distribution. Because the unpolarized antiquark distribution functions have been determined well from global analyses, there are strong constraints on the  $x$  dependence of the GPDs  $H$  for antiquarks. Therefore, the GK GPDs contain the sea-quark component in addition to the valence-quark and gluon GPDs. It is the reason why there are finite distributions at  $x < -\xi = -0.15$  in the function  $H^q$ . On the other hand, there is little information on sea-

quark GPDs on other functions  $\tilde{H}$ ,  $E$ , and  $\tilde{E}$ . Therefore, the GK parametrization supplies only the valence-quark GPDs for the quark part in these GPDs, which indicates that the quark GPDs are zero at  $x < -\xi = -0.15$  as clearly shown in Fig. 4. Because of this, there are sudden changes at  $x = -\xi = -0.15$  in the quark GPDs  $\tilde{H}^q$ ,  $E^q$ , and  $\tilde{E}^q$ .

We also notice that the pion- and rho-pole contributions are large in all the GPDs of  $H$ ,  $E$ , and  $\tilde{E}$  in Fig. 4. In particular, the pion-pole effects are much larger than other GPD distributions in  $\tilde{E}$ , and the rho-pole effects are much larger than other distributions in  $E$ . The rho-pole effects are comparable in magnitude to the other distributions in  $H$ . These facts indicate that the understanding of the meson contributions is important for clarifying the GPDs in the whole kinematical region.

As for the gluon GPDs, the unpolarized gluon distribution is relatively well determined, so that there are constraints on the  $x$  distribution part of the gluon GPD  $H^g$ . However, the longitudinally-polarized gluon distribution still has a large uncertainty and it cannot be fixed in the current global analysis. Therefore, although  $\tilde{H}^g$  distribution of Fig. 4 is supplied in the GK parametrization, it could have a large uncertainty. As for the gluon GPD  $E^g$ , there is little information, so that its distribution should be considered as an undermined quantity at this stage although  $E^g$ , which is the variant 3 of the GK-2009 paper [46], is shown in Fig. 4. The  $E^g$  distribution is much smaller than other quark GPDs  $E^{u,d}$ . There is no  $\tilde{E}^g$  in the GK parametrization at this stage.



## B. Cross sections for the $\pi^+$ production

First, we show the  $\pi^+$  production cross section by using the GK GPDs of Sec. III A. The same kinematical condition of Ref. [33] is taken for calculating the cross section, because the condition could be realized roughly in the Fermilab experiment with the 10 GeV neutrino beam. Namely, we take  $s = 20 \text{ GeV}^2$ ,  $y = 0.7$ , and  $\Delta_T = 0$ . This choice of  $\Delta_T = 0$  means that the momentum-transfer squared  $t$  is expressed by  $\xi$  as follows. From Eq. (3), the variable  $t$  is expressed in terms of  $\xi$  and the transverse component of the momentum transfer  $\Delta_T$  and it becomes  $t = -4\xi^2 m_N^2 / (1 - \xi^2) + \Delta_T^2 / (1 - \xi^2) = -4\xi^2 m_N^2 / (1 - \xi^2)$  if  $\Delta_T^2 = -\tilde{\Delta}_T^2 = 0$ . Later in this subsection, the  $s$  dependence of the cross section is shown by taking also  $s = 30$  and  $100 \text{ GeV}^2$ .

The  $\nu + p \rightarrow \ell^- + p' + \pi^+$  cross section is shown in Fig. 5 as the function of  $Q^2$  from  $2 \text{ GeV}^2$  to  $6 \text{ GeV}^2$ . Three curves are shown. The solid curve indicates the cross section with the whole quark and gluon GPD contributions, the dashed does the gluon GPD contribution by terminating the quark GPDs ( $C_q = 0$ ), and the dot-dashed does the quark GPD contribution by terminating the gluon GPDs ( $C_g = 0$ ). We notice that the whole cross section is dominated by the gluon GPD terms. This gluon dominance is roughly understood as follows. Let us consider the kinematical factors in the quark and gluon contributions. In the cross section of Eq. (39), there are coefficients  $C_q$  and  $C_g$  in front of the quark and gluon Compton form factors, which contain the factors  $2f_\pi$  and  $8f_\pi/\xi$  and the integrals of pion distribution amplitude in Eq. (33). The ratio of these factors are

$$\frac{\xi C_q}{8C_g} = 0.05 - 0.19 \quad \text{for } y = 0.7 \quad (46)$$

from  $Q^2 = 2 \text{ GeV}^2$  to  $6 \text{ GeV}^2$ . In Fig. 5, the quark GPD contributions to the cross sections are one order of magnitude smaller than the gluon GPDs ones, which roughly corresponds this ratio. However, the functional forms are different between the quark and gluon GPDs, which leads

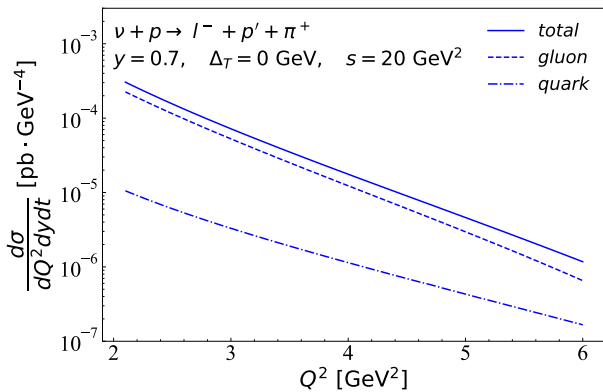


FIG. 5.  $\pi^+$ -production cross sections for  $\nu p \rightarrow \ell^- p' \pi^+$  at  $y = 0.7$ ,  $\Delta_T = 0 \text{ GeV}$ , and  $s = 20 \text{ GeV}^2$ .

to another factor in estimating the precise quark-gluon contribution ratio.

In order to find which GPDs will be determined from the neutrino reactions, we show each component contribution to the  $\pi^+$  cross section in Fig. 6. Namely, the cross sections are shown from

- (1) quark GPD terms of  $H^q$  and  $E^q$ :  
 $|\mathcal{H}^q|^2, |\mathcal{E}^q|^2, \mathcal{H}^q \mathcal{E}^{q*},$
- (2) quark GPD terms of  $\tilde{H}^q$  and  $\tilde{E}^q$ :  
 $|\tilde{\mathcal{H}}^q|^2, |\tilde{\mathcal{E}}^q|^2, \tilde{\mathcal{H}}^q \tilde{\mathcal{E}}^{q*},$
- (3) gluon GPD terms of  $H^g$  and  $E^g$ :  
 $|\mathcal{H}^g|^2, |\mathcal{E}^g|^2, \mathcal{H}^g \mathcal{E}^{g*},$
- (4) quark-gluon interference terms:  
 $\mathcal{H}^q \mathcal{H}^{g*} + \mathcal{H}^g \mathcal{H}^{q*}, \mathcal{E}^q \mathcal{E}^{g*} + \mathcal{E}^g \mathcal{E}^{q*},$   
 $\mathcal{H}^q \mathcal{E}^{g*}, \mathcal{H}^g \mathcal{E}^{q*},$

for the  $\pi^+$ -production cross section.

First, the largest contribution comes from the gluon GPD  $H^g$  as shown in the curve of  $|\mathcal{H}^g|^2$ , whereas the  $E_g$  term  $|\mathcal{E}^g|^2$  is much smaller than the leading  $|\mathcal{H}^g|^2$ . Their interference  $\mathcal{H}^g \mathcal{E}^{g*}$  is typically one order of magnitude smaller than  $|\mathcal{H}_g|^2$ . It means that the  $\pi^+$  cross section is mainly sensitive to the gluon GPD  $H^g$ . As shown in Eq. (39), there is no term from the polarized GPDs  $\tilde{H}^g$  and  $\tilde{E}^g$ . These results depend, of course, on the employed GPDs. In particular, the gluon GPD  $E^g$  is weakly constrained in the current parametrization and it should have larger uncertainty even in the overall magnitude.

Second, the pure quark-term contributions are one or two orders of magnitude smaller than the gluon ones. For example, the  $|\mathcal{H}^q|^2$  cross section is one order of magnitude smaller than the leading  $|\mathcal{H}^g|^2$  one. In the same way with the gluon case, the  $|\mathcal{E}^q|^2$  is much smaller than  $|\mathcal{H}^q|^2$ , so the leading quark contribution comes from  $H^q$ . The polarized quark GPDs' contributions are about one order of magnitude smaller than the corresponding unpolarized quark GPDs. For example, the  $|\tilde{\mathcal{H}}^q|^2$  cross section is one order of magnitude smaller than the leading  $|\mathcal{H}^q|^2$  one. The  $|\tilde{\mathcal{E}}^q|^2$  cross section is further smaller than the  $|\tilde{\mathcal{H}}^q|^2$  one.

Third, the quark-gluon interference contributions are between the pure quark and gluon cross sections in magnitude. Among the terms, the GPD term  $\mathcal{H}^q \mathcal{H}^{g*} + \mathcal{H}^g \mathcal{H}^{q*}$  is the largest one, the next one is  $\mathcal{H}^g \mathcal{E}^{q*}$ , and then  $\mathcal{H}^q \mathcal{E}^{g*}$ . The  $\mathcal{E}^q \mathcal{E}^{g*} + \mathcal{E}^g \mathcal{E}^{q*}$  term is the smallest in the interference. From these discussions, we roughly list the GPDs from the largest as

$$(1) H^g \quad (2) H^q \quad (3) \tilde{H}^q \quad (4) E^q, \tilde{E}^q, E^g, \quad (47)$$

for the  $\pi^+$  production. In the  $\pi^0$  production, the gluon GPDs do not contribute as the leading one as discussed later in this section.

As shown in Fig. 5 and also later in Fig. 12, the fraction of the quark-GPD contribution increases at large  $Q^2$ . This tendency is understood from Fig. 6, where the

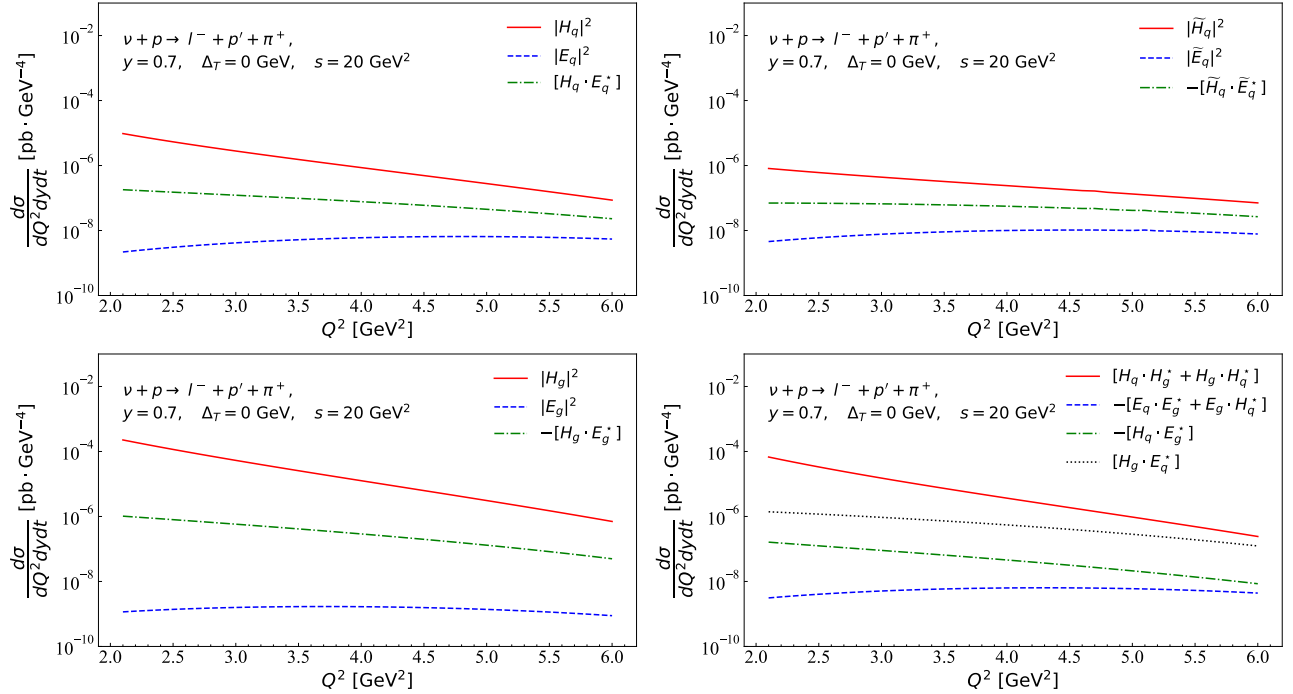


FIG. 6. Each component of the  $\pi^+$ -production cross section for  $\nu p \rightarrow \ell^- p' \pi^+$ .

gluon- $H$  term drops more rapidly as increasing  $Q^2$  than quark- $H$  term does mainly due to the kinematical factor  $\xi$  given in Eq. (46). The ratio of Eq. (46) increases from 0.05 at  $Q^2 = 2 \text{ GeV}^2$  to 0.19 at  $Q^2 = 6 \text{ GeV}^2$ . In addition, there are effects from the difference between the functional forms of  $H_g$  and  $H_q$ . We also notice that the  $Q^2$  dependencies of other terms are different between gluon and quark contributions.

Another interesting point of the GPD determination is on the role of the GPDs in the ERBL region. After Eq. (36), we mentioned that the cross section is sensitive to the GPDs of the ERBL region. However, such effects need to be clarified numerically for proposing neutrino GPD experiments. Although the ERBL is an important kinematical region, its GPDs have not been determined experimentally. An ERBL-GPD investigation is under consideration, for example, at J-PARC by the  $N + N \rightarrow \pi + N + B$  reactions [12–14]. We need more studies whether the GPDs in the ERBL region could affect the neutrino-induced pion-production cross sections and also deeply virtual meson production (DVMP) ones of the charged-lepton reactions.

Using the pion- and rho-pole GPDs

$$\tilde{E}_\pi, H_\rho, E_\rho,$$

in Eqs. (27) and (29), we calculated their effects on the  $\pi^+$  cross section. The results are shown in Fig. 7 by terminating the gluon GPDs in order to clarify these pole-term contributions. Four curves are shown by taking the following four types of the GPDs:

- (1) GPDs with the pion and rho poles,
- (2) GPDs with only the pion pole,

- (3) GPDs with only the rho pole,
- (4) GPDs without pion and rho poles.

The pion-pole GPDs ( $\tilde{E}_\pi^{u,d}$ ) increase the cross section slightly in Fig. 7. On the other hand, the rho-pole GPD ( $H_\rho^{u,d}, E_\rho^{u,d}$ ) effects are large and they increase the cross section significantly. It simply comes from the fact that the  $H^q$  effects are much larger than the  $\tilde{E}^q$  ones in the cross section as shown in Eq. (47). In fact, the quark GPDs  $H^q$  are significantly modified if the rho-pole GPDs are added as shown in Fig. 4. The rho- and pion-pole effects are much larger in  $E^q$  and  $\tilde{E}^q$ , respectively, in Fig. 4; however, their modifications do not appear clearly in the cross section simply because the fractions of  $E^q$  and  $\tilde{E}^q$  are small in the cross section. In any case, because the pion production cross section is sensitive to the GPDs

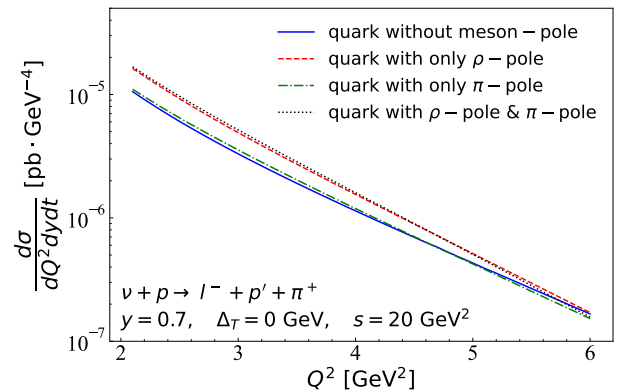


FIG. 7. Pion- and rho-pole effects on the  $\pi^+$  cross section for  $\nu p \rightarrow \ell^- p' \pi^+$  by terminating the gluon GPDs.

in the ERBL region, the detailed GPD studies in a wide kinematical region could become possible by investigating the neutrino reactions in addition to the charged-lepton reactions. In general, the pure quark-GPD contributions are about one order of magnitude smaller than the pure-gluon GPD ones. However, the quark-gluon interference contributions are not so small as shown in the lower-right figure of Fig. 6, so that the meson-pole effects may appear in measured  $\pi^+$ -production cross sections. These effects should be more pronounced in the  $\pi^0$  production in Sec. III C because the gluon contribution does not exist.

The pion-pole term is included in the GK parametrization [38, 47], and the GPD constraints are satisfied with this term. For example, the first moment of the pion-pole term becomes the pseudoscalar form factor as shown in Eq. (35) of Ref. [48]. The pion-pole term could contribute to the DVCS; however, it is very small due to the small  $\pi^0\gamma\gamma$  coupling [49]. We need to make a new global analysis in principle if the rho-pole term is included in the GPDs for the accurate determination of the GPDs because the rho-pole term is not included in the GK parametrization. We consider it as a future project. At this stage, we simply added the rho-pole term to the existing GPD parametrization in order to find its effects on the neutrino cross section. One may note that there is not much freedom in the meson-pole terms of Eqs. (27) and (29), although the  $t$ -dependent form factor could deviate from the dipole forms at large  $|t|$ . Therefore, we think that such pole terms exist in the close forms of Eqs. (27) and (29). However, such additional rho-pole GPD terms contribute also the DVMP cross sections in charged-lepton scattering, so that the whole GPDs should be readjusted by a new global analysis.

In the unpolarized collinear PDFs, the pion- and rho-cloud contributions could be calculated, for example, in discussing a possible model to explain  $\bar{u} - \bar{d}$  and the Gottfried-sum-rule violation [50]. However, the global-analysis PDFs have certain  $x$ -dependent function forms with parameters, and the meson-cloud effects are effectively included in the PDFs. In the same way, the rho-pole GPDs should be included within the GPD functions in future global analyses. Currently, the GPD global analysis is at the transition stage in the sense the pion-pole GPDs are separately defined in the GK parametrization. In our work, the rho-pole GPDs are separately treated in the similar way. In future, the whole GPDs should be determined without relying on a specific model.

Next, we show the effect of the gluon GPD  $E^g$  on the cross section because the  $\pi^+$  production is sensitive to the gluon GPDs. However, the gluon GPD  $E^g$  could be small in comparison with the quark ones  $E^u$  and  $E^d$  as already shown in Fig. 4. In the GK parametrization of 2009 [46], the six types, variants 1, 2,  $\dots$ , 6, are prepared as different functional forms of  $E^g$ . Among them, we take the variants 1, 2, and 3 as three extreme cases for

$E^g$ , and they are shown in Fig. 8 in comparison with the quark GPDs  $E^{u,d}$ , where the rho-pole GPDs of Fig. 4 are not included. In the PARTONS code [2], the GPD  $E^g$  of the variant 3 is given.

Although the gluon GPD  $H^g$  is as large as the quark GPDs  $H^q$  as shown in Fig. 4, the situation is very different for the GPDs  $E^{q,g}$ . The gluon GPD  $E^g$  is expected to be much smaller than the quark GPDs  $E^q$  [46]. The gluon GPD  $E^g$  is parametrized as  $E^g(x, \xi = 0, t = 0) \equiv e_g(x) = N_g x^{-\alpha_g} (1-x)^{\beta_g}$  in the forward limit  $\xi = t = 0$ , and the same functional forms are used also for the valence-quark and antiquark GPDs [ $e_{q_v}(x)$  and  $e_{\bar{q}}(x)$ ]. The overall magnitudes of the valence-quark functions  $e_{u_v}(x)$  and  $e_{d_v}(x)$  are constrained by the Pauli form factors, namely the anomalous magnetic moments ( $\kappa_{p,n}$ ), of the proton and neutron as  $\kappa_{u,d} = \int_0^1 dx e_{u_v,d_v}(x)$ , where  $\kappa_u = 2\kappa_p + \kappa_n$ ,  $\kappa_d = \kappa_p + 2\kappa_n$  [51]. From the conservations of the momentum and total angular momentum, we have the sum rule [46, 52]

$$\int_0^1 dx x e_g(x) = - \sum_q \int_0^1 dx x [e_{q_v}(x) + 2e_{\bar{q}}(x)], \quad (48)$$

for constraining the gluon part. However, the analysis of the Pauli form factors indicated that the  $e_{u_v}(x)$  and  $e_{d_v}(x)$  distributions almost cancel with each other [51], which could lead to a small distribution of  $e_g(x)$  in comparison with the overall magnitudes of  $e_{u_v}(x)$  and  $e_{d_v}(x)$  although the magnitude of the gluon function  $e_g(x)$  still depends on the antiquark functions  $e_{\bar{q}}(x)$ . This situation is similar in the updated analysis of 2020 [53], and  $e_g(x)$  of the 2020 version is within the range between the variants 2 and 3 in Fig. 8.

In order to show the variations of the cross section from the gluon GPD  $E^g$ , we take three GPD models, variants 1, 2, and 3, in the GK parametrization of 2009 [46]:

$$\text{Variant 1: } e_g(x) = 0,$$

$$\text{Variant 2: } e_g(x) = -0.873 x^{-1.1} (1-x)^6,$$

$$\text{Variant 3: } e_g(x) = 0.776 x^{-1.1} (1-x)^6.$$

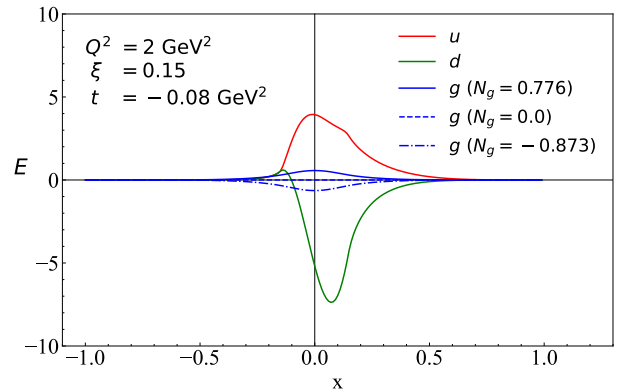


FIG. 8. The GPDs  $E^{u,d,g}$  of the GK parametrization by taking the variants 1, 2, and 3 for  $E^g$  at  $Q^2 = 2 \text{ GeV}^2$ ,  $\xi = 0.15$ , and  $t = -0.08 \text{ GeV}^2$ . Here, the rho-pole terms are not included in the quark GPDs.

The Diehl-Kugler model-1 [52] and the Kroll-2020 model [53] for  $E^g$  are smaller in magnitude than the  $E^g$  of the GK-variants 2 and 3. In Fig. 8, these GK GPDs  $E^g$  are shown with the quark GPDs at  $Q^2 = 2 \text{ GeV}^2$ ,  $\xi = 0.15$ , and  $t = -0.08 \text{ GeV}^2$ . Here, the rho-pole terms are not included in showing the quark GPDs, so that they are the original GK quark GPDs. We find that the  $E^g$  variations are small in comparison with the quark GPDs.

Using these GK GPDs  $E^g$ , we calculated the  $\pi^+$  cross sections and they are shown in Fig. 9. The effects of the  $E^g$  is very small in the  $\pi^+$  cross section, simply because the magnitude of  $E^g$  is much smaller than other GPDs  $H^{g,q}$  and even than  $E^q$ . In the  $\pi^+$  cross section, the quark term  $E^d(x, \xi, t) - E^u(-x, \xi, t)$  contributes as shown in Eq. (34). Therefore,  $E^d$  and  $-E^u$  additively contribute to the cross section, which makes the  $E^g$  fraction even smaller. Therefore, it is difficult to find the gluon  $E^g$  from the pion-production process in neutrino scattering. In the pion-production measurements with unpolarized targets, the GPD  $\tilde{H}$ ,  $\tilde{E}$  and  $E$  contributions are very small. For determining these GPDs, we should rely, for example, on vector-meson productions with polarized targets [46, 47].

In Fig. 10, the  $\pi^+$ -production cross sections are shown for  $\nu p \rightarrow \ell^- p' \pi^+$  by varying the center-of-mass energy squared as  $s = 20, 30$ , and  $100 \text{ GeV}^2$ . The cross section is very sensitive to the neutrino beam energy, and the reaction  $\nu p \rightarrow \ell^- p' \pi^+$  cross section increases with the increasing energy. The flux factor  $\bar{F}$  of Eq. (38) decreases with the increasing  $s$ . However, the longitudinal cross section  $\sigma_L$  of Eq. (39) increases more rapidly with  $s$  by the following reason. The increase of  $s$  means the decrease of  $x$  and  $\xi$ , so that the smaller  $x$  and  $\xi$  regions of the GPDs contribute to the integrals in Eq. (33). In the reaction  $\nu p \rightarrow \ell^- p' \pi^+$ , the gluon GPDs dominate the cross section. As  $x$  becomes smaller, the gluon GPDs increase rapidly, which leads the larger cross sections with increasing  $s$ .

The single differential cross section  $d\sigma/dy$  is shown for the process  $\nu p \rightarrow \ell^- p \pi^+$  by integrating the cross section

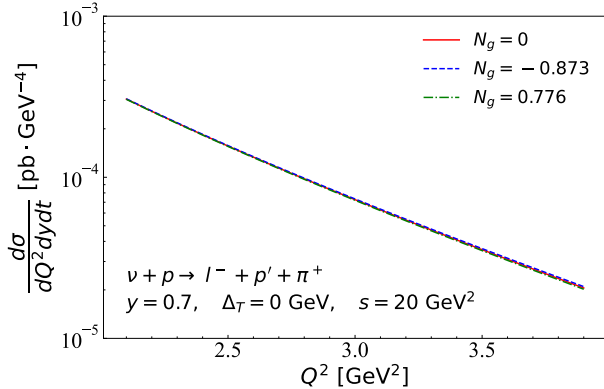


FIG. 9.  $E^g$  effects on the  $\pi^+$  production cross section for  $\nu p \rightarrow \ell^- p' \pi^+$  by taking three GK  $E^g$  models of the variants 1, 2, and 3.

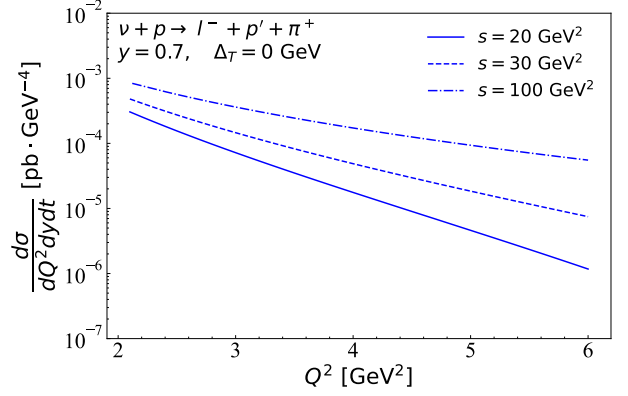


FIG. 10. Center-of-mass-energy squared dependence of the  $\pi^+$ -production cross section for  $\nu p \rightarrow \ell^- p' \pi^+$  by taking  $s = 20, 30$ , and  $100 \text{ GeV}^2$ .

over  $Q^2$  and  $t$  at  $s = 20, 30$ , and  $100 \text{ GeV}^2$  in Fig. 11. The cross section is about  $4 \times 10^{-5} - 5 \times 10^{-4} \text{ pb}$  at  $y = 0.4 - 0.5$ , and it becomes smaller with increasing  $y$ . The minimum value of  $Q^2$  ( $Q_{\min}^2$ ) for the integral is taken as  $Q_{\min}^2 = 2 \text{ GeV}^2$ . The cross section varies depending on  $Q_{\min}^2$ , for example,  $d\sigma/dy = 3.7 \times 10^{-5}, 4.0 \times 10^{-6}, 4.2 \times 10^{-7} \text{ pb}$  for  $Q_{\min}^2 = 2, 3, 4 \text{ GeV}^2$ , respectively, at  $y = 0.4$  and  $s = 20 \text{ GeV}^2$ . The  $y$  dependence of the cross section is contained mainly in the longitudinal photon polarization  $\varepsilon$  above Eq. (38) as  $2(1 - y)$  at large  $y$  and in the  $\bar{F}$  of Eq. (38) as  $1/y$ , so that the cross sections decrease with increasing  $y$  in general. The variable  $y$  is related to  $x$  and  $Q^2$  as  $y = Q^2/[x(s - m_N^2)]$ , so that  $x$  dependence of the GPDs also affect.

The cross section for  $\pi^+$  production from the neutron ( $\nu n \rightarrow \ell^- n' \pi^+$ ) is also calculated in the same way by exchanging the GPDs  $F^u$  and  $F^d$  from the proton-target case due to the isospin symmetry. Its cross section is shown in Fig. 12 by showing the quark and gluon GPD contributions and their total. The result are similar to the cross sections in Fig. 5 for the reaction  $\nu p \rightarrow \ell^- p' \pi^+$ . The cross section is dominated by the gluon terms; however, there is a tendency that the fraction of the quark-

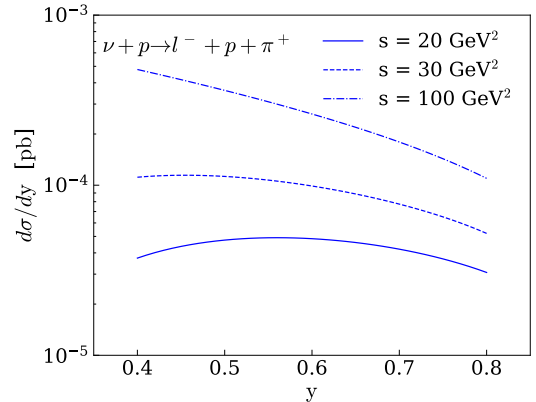


FIG. 11. Single differential cross section  $d\sigma/dy$  is shown for  $\nu p \rightarrow \ell^- p \pi^+$  by taking  $s = 20, 30$ , and  $100 \text{ GeV}^2$ .

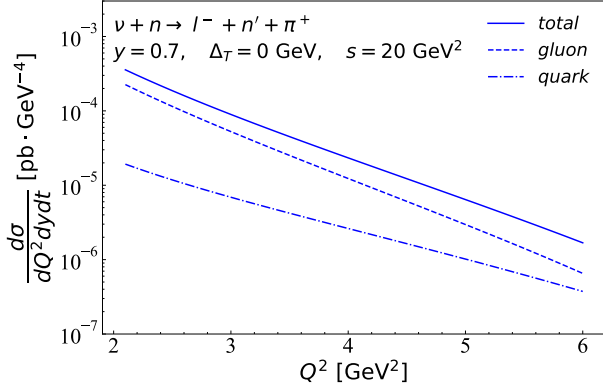


FIG. 12.  $\pi^+$ -production cross sections for  $\nu n \rightarrow \ell^- n' \pi^+$  at  $y = 0.7$ ,  $\Delta_T = 0$  GeV, and  $s = 20$  GeV $^2$ .

GPD contribution increases at large  $Q^2$  as noted in Fig. 5.

At the Fermilab,  $\nu_\mu$  and  $\bar{\nu}_\mu$  scattering experiments are possible with the hydrogen (H) and nuclear (A) targets by using the high-intensity LBNF beam [19, 20]. Using the proton target H, we could investigate the pion-production processes

$$p: \nu_\mu p \rightarrow \mu^- p \pi^+, \quad \bar{\nu}_\mu p \rightarrow \mu^+ p \pi^-, \quad \bar{\nu}_\mu p \rightarrow \mu^+ n \pi^0.$$

If a nuclear target A, such as carbon and argon, is used, it is possible to access the additional reactions with the neutron:

$$n: \nu_\mu n \rightarrow \mu^- n \pi^+, \quad \nu_\mu n \rightarrow \mu^- p \pi^0, \quad \bar{\nu}_\mu n \rightarrow \mu^+ n \pi^-,$$

where nuclear corrections should be applied properly. Because of the isospin symmetry, we expect that the neutron cross sections are related to the proton cross sections theoretically as

$$\text{Fig. 5: } \sigma(\bar{\nu}_\mu n \rightarrow \mu^+ n \pi^-) = \sigma(\nu_\mu p \rightarrow \mu^- p \pi^+),$$

$$\text{Fig. 12: } \sigma(\nu_\mu n \rightarrow \mu^- n \pi^+) = \sigma(\bar{\nu}_\mu p \rightarrow \mu^+ p \pi^-),$$

$$\text{Fig. 13: } \sigma(\nu_\mu n \rightarrow \mu^- p \pi^0) = \sigma(\bar{\nu}_\mu p \rightarrow \mu^+ n \pi^0), \quad (49)$$

where the corresponding numerical results are shown in Figs. 5, 12, and 13. The third cross section  $\sigma(\nu_\mu n \rightarrow \mu^- p \pi^0)$  is discussed in the next subsection. Using these cross sections, we can estimate all the reaction cross sections numerically for the pion ( $\pi^\pm$ ,  $\pi^0$ ) productions in the neutrino and antineutrino reactions at Fermilab by taking into account nuclear modifications if the target is a nucleus. We also mention that the transverse form factor component of the GPD  $\tilde{H}^q$  is constrained by the axial form factor measured in neutrino reactions, for example, by the recent MINER $\nu$ A experiment [54].

### C. Cross sections for the $\pi^0$ production

Next, we discuss the  $\pi^0$ -production cross section in neutrino scattering. Here, the cross section is sensitive to the quark GPD combination  $[\{F^u(x, \xi, t) - F^d(x, \xi, t)\} +$

$\{F^u(-x, \xi, t) - F^d(-x, \xi, t)\}]/\sqrt{2}$  as shown in Eq. (35). In the charged-current neutrino scattering, there is no leading-gluon term, as shown in Fig. 3, for the  $\pi^0$  production because of the charge conservation  $W^\pm \not\leftrightarrow \pi^0$ . Therefore, it is suitable for determining the quark GPDs. Furthermore, the pion- and rho-pole GPDs are symmetric under the transformation  $x \rightarrow -x$  as obvious in Eqs. (27) and (29), there are pion and rho-pole GPD contributions ( $[\{F^u(x, \xi, t) - F^d(x, \xi, t)\} + \{F^u(-x, \xi, t) - F^d(-x, \xi, t)\}]_{\pi, \rho\text{-poles}}/\sqrt{2}$ ) to the cross section. It means that the  $\pi^0$ -production could be suitable for determining the quark GPDs including the pion- and rho-pole terms.

Calculated  $\pi^0$  cross sections for the process  $\nu + n \rightarrow \ell^- + p + \pi^0$  are shown in Fig. 13 by taking the kinematical conditions,  $\Delta_T = 0$  GeV and  $s = 20$  GeV $^2$ . Three curves are shown for  $y = 0.3, 0.5$ , and  $0.7$ . The largest contribution comes from the GPDs  $H^q$ , and subsequent one is  $\tilde{H}^q$ , and then  $E^q$  and  $\tilde{E}^q$  in order as the same way with the  $\pi^+$  production. Here, the pion- and rho-pole terms are not included.

Next, including the pion- and rho-pole GPD contributions, we show the  $\pi^0$  cross sections for the process  $\nu + n \rightarrow \ell^- + p + \pi^0$  by taking  $y = 0.7$ ,  $\Delta_T = 0$  GeV and  $s = 20$  GeV $^2$  in Fig. 14. Four cross sections are shown. The solid curve indicates the cross section

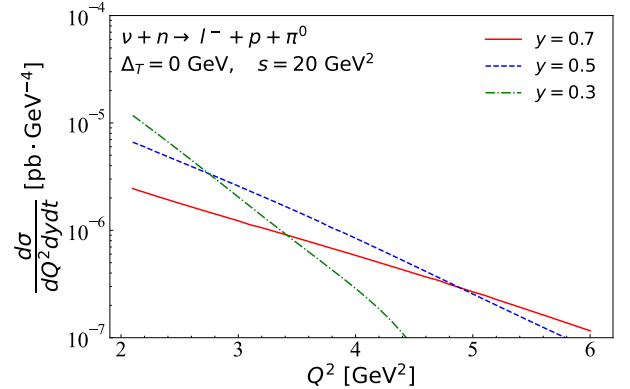


FIG. 13.  $\pi^0$  production cross sections for  $\nu n \rightarrow \ell^- p \pi^0$  at  $\Delta_T = 0$  GeV and  $s = 20$  GeV $^2$ .

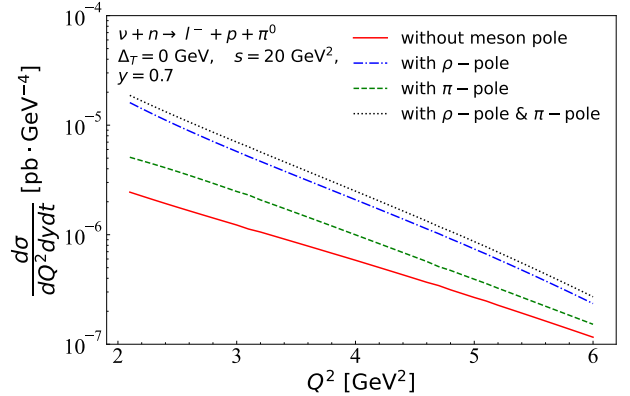


FIG. 14. Pion- and rho-pole effects on the  $\pi^0$  production cross section for  $\nu n \rightarrow \ell^- p \pi^0$  at  $y = 0.7$ ,  $\Delta_T = 0$  GeV and  $s = 20$  GeV $^2$ .

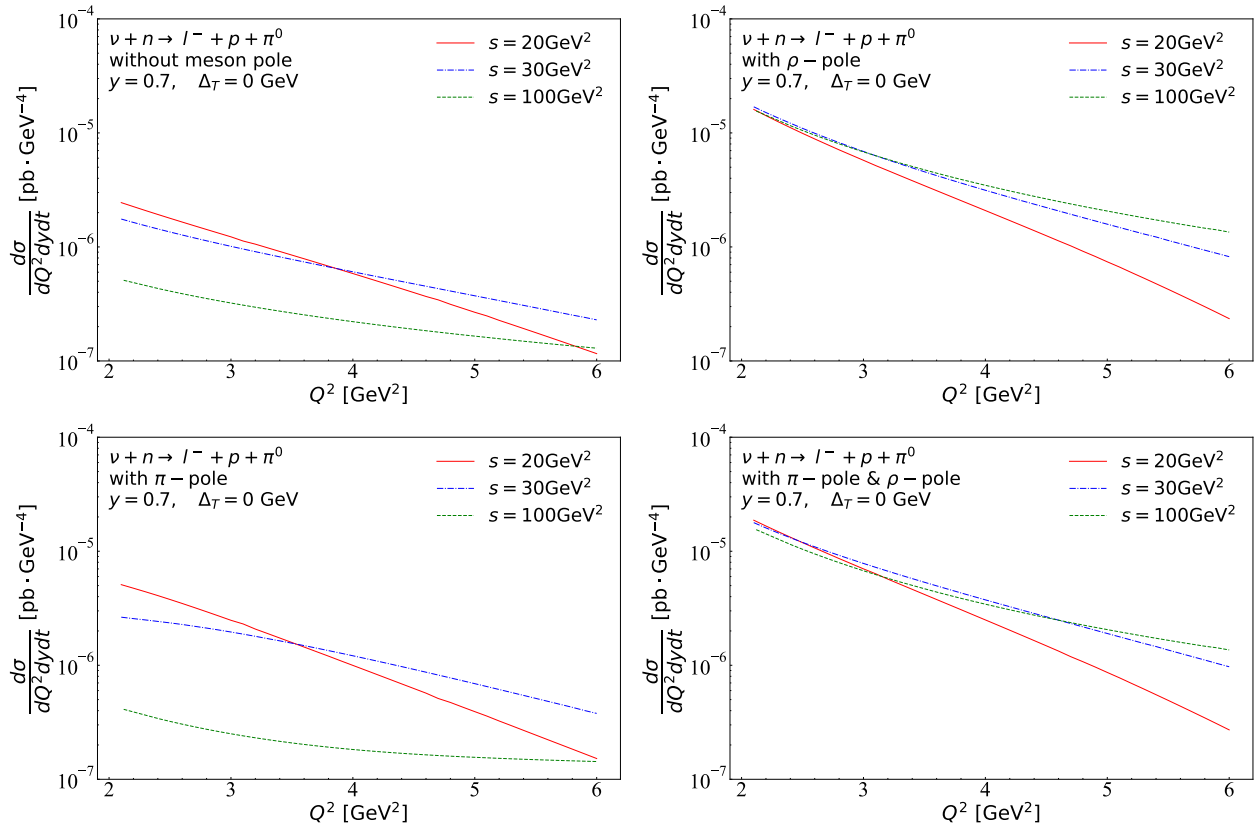


FIG. 15. Center-of-mass-energy squared dependence of the  $\pi^0$ -production cross section for  $\nu n \rightarrow \ell^- p \pi^0$  by taking  $s = 20, 30$ , and  $100 \text{ GeV}^2$  with or without the pion- and rho-pole GPDs.

without the pion and rho-pole GPDs, the dashed curve does the one by including only the pion-pole GPDs, the dashed-dot curve does by including only the rho-pole GPDs, and the dotted curve does by including the pion and rho-pole GPDs. It is obvious that the pion- and rho-pole effects increase the  $\pi$ -production cross section significantly. The increase is much larger by adding the rho pole than the pion pole. It is simply because the rho-pole GPDs exist in the function  $H$ , which is the largest component in the pion-production cross sections. In this way, we found that the pion- and rho-pole GPDs could be studied in the  $\pi^0$  production process. However, such pronounced meson-pole GPD effects should be re-estimated by a new global analysis including the data of charged-lepton scattering as we mentioned in Sec. III B. The GPDs in the ERBL region, namely the meson-pole terms, have never been investigated experimentally, but they could be studied by the neutrino reactions, especially by the  $\pi^0$  production processes. These reactions are totally different from the hadronic reaction under consideration at J-PARC for probing the ERBL region [12–14].

The energy dependence of the  $\nu n \rightarrow \ell^- p \pi^0$  cross section is shown in Fig. 15 by taking  $s = 20, 30$ , and  $100 \text{ GeV}^2$  with or without the pion- and rho-pole GPDs. Without the meson-pole GPDs, the cross section decreases with increasing  $s$  as shown in the upper-left figure

as a general tendency, although the details depends also on  $Q^2$  as the  $s = 30 \text{ GeV}^2$  cross section becomes larger than the  $s = 20 \text{ GeV}^2$  one at large  $Q^2$ . This general tendency is opposite to the increasing cross section of  $\nu p \rightarrow \ell^- p' \pi^+$  with  $s$  in Fig. 10. It is because the quark GPDs do not increase as rapidly as the gluon GPDs as  $x$  decreases with the increasing  $s$ . This energy dependence stays the same even if the pion-pole GPDs are added as shown in the lower-left figure, although the overall cross sections become larger at  $s = 20$  and  $30 \text{ GeV}^2$ . If the rho-pole GPDs are added as shown in the upper- and lower-right figures, the cross sections become much larger and the energy dependence is much different. As  $s$  increases to  $s = 30$  and  $100 \text{ GeV}^2$ , the cross section becomes much larger than the one of  $s = 20 \text{ GeV}^2$ , especially in the large  $Q^2$  region. The difference between the pion- and rho-pole GPD effects comes from the fact that the rho-pole GPDs exist in the main component  $H^q$  (and subleading one  $E^q$ ) and the pion-pole GPDs are in the subleading  $\tilde{E}^q$  in the cross section. These results indicate again that the neutrino reactions could be used for probing the ERBL region of the GPDs.

As seen in the cross-section figures, the cross sections are shown in the  $Q^2$  range from  $2 \text{ GeV}^2$  to  $6 \text{ GeV}^2$ . In the low  $Q^2$  region at  $Q^2 \sim 2 \text{ GeV}^2$ , there could be significant corrections due to higher-twist and higher-order- $\alpha_s$  effects. For example, it is interesting to include the these

effects in Eq. (33) in the sense that the cross section becomes sensitive to the functional form of the pion distribution amplitude  $\Phi_\pi(x)$  as shown in Ref. [29]. In the cross sections integrated over  $\phi$ , the higher-twist terms  $\sigma_{TT}$  and  $\sigma_{LT}$  does not contribute. In the unintegrated pion-production cross sections in the charged-lepton scattering, the higher-twist effects were calculated and they are sizable magnitude at small  $Q^2(=1-2 \text{ GeV}^2)$  in comparison with the leading-twist effects [16, 27, 55]. In fact, an analysis result for the pion electroproduction cross sections indicates that the higher-twist contributions could be comparable to the leading one in magnitude at  $Q^2 = 2 \text{ GeV}^2$  and  $s = 20 \text{ GeV}^2$ . The cross sections  $\sigma_{TT}$  and  $\sigma_{LT}$  are expressed by the transversity GPDs [16, 27, 55]; however, there is no study on the meson-pole effects on the transversity GPDs as far as we are aware. Because the  $\sigma_{TT}$  and  $\sigma_{LT}$  are sizable in magnitude at small  $Q^2$ , it could be important to include the meson-pole effects also on the transversity GPDs in future analysis.

The single differential cross section  $d\sigma/dy$  is shown for the process  $\nu n \rightarrow \ell^- p \pi^0$  by integrating the cross section over  $Q^2$  and  $t$  at  $s = 20, 30$ , and  $100 \text{ GeV}^2$  in Fig. 16. The cross section is about  $1 \times 10^{-6} - 4 \times 10^{-6} \text{ pb}$  at  $y = 0.4 - 0.5$ .

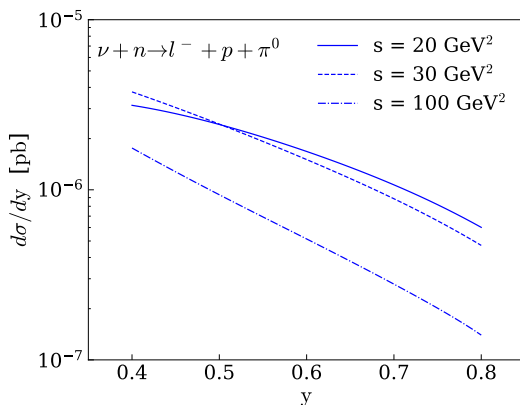


FIG. 16. Single differential cross section  $d\sigma/dy$  is shown for  $\nu n \rightarrow \ell^- p \pi^0$  by taking  $s = 20, 30$ , and  $100 \text{ GeV}^2$ .

In general, neutrino DIS measurements have been valuable in determining light-quark flavor-dependent distributions, the valence-quark distributions, and the strange-quark distribution. The situation could be same for the GPD determination, and future neutrino reaction experiments will provide valuable information on the gluon GPDs and also the quark GPDs, especially on the flavor dependence. One may note that it is not easy to achieve precise measurements in neutrino reactions because the neutrino beam has a wide energy distribution instead of the monochromatic one in the charged-lepton beam. However, a detector with a wide angular acceptance and a low-momentum threshold could make it possible to investigate the GPDs in the neutrino reactions [22]. Although there is no experiment for the GPDs in neutrino scattering, such a project is under consideration at Fermilab [20] by using the high-energy neutrino beam of about  $10 \text{ GeV}$  [19], and it may be possible also at the

nuSTORM [21, 22]. We hope that these experimental projects will be realized and that it will lead to a better understanding on the GPDs.

#### IV. SUMMARY

We investigated the pion-production processes in neutrino reactions for determining the nucleon GPDs. Using the GK parametrization for the GPDs, we showed the effects of the gluon and quark GPDs in the process  $\nu + p \rightarrow \ell^- + p' + \pi^+$ . The largest contribution to the  $\pi^+$  production comes from the GPD  $H^g$ , then subsequent contributions are  $H^q$ ,  $\tilde{H}^q$ , and  $E^q$ ,  $\tilde{E}^q$ ,  $E^g$  in order by showing each term in the cross section. The pion-pole GPDs are large in the function  $\tilde{E}$ , and the rho-pole GPDs exist as large components in the functions  $H$  and  $E$ . We showed these-pole effects in the  $\pi^+$ -production cross sections. We found that the GPD  $E^g$  effects are small in the  $\pi^+$ -production cross section according to the current parametrization for  $E^g$ . In the  $\pi^0$  production  $\nu + n \rightarrow \ell^- + p + \pi^0$ , the quark GPDs can be investigated. In particular, the pion- and rho-pole contributions are large in the  $\pi^0$  cross section, which indicates that this process could be used for finding the GPDs in the ERL region. However, the additional rho-pole GPDs should be tested by a new global analysis with the charged-lepton data. We also showed the dependence of the cross sections on the center-of-mass energy squared by calculating the cross sections at  $s = 20, 30$ , and  $100 \text{ GeV}^2$ . As  $s$  increases, the  $\nu + p \rightarrow \ell^- + p' + \pi^+$  cross section increases, whereas the  $\nu + n \rightarrow \ell^- + p + \pi^0$  one decreases or increases with  $s$ , depending mainly on the meson-pole GPDs and also on  $Q^2$ . This difference between the two processes comes from the difference between the gluon and quark GPDs as  $x$  decreases. In general, the gluon GPDs increase more rapidly than the quark GPDs as  $x$  becomes smaller. Future neutrino GPD projects will be valuable also for finding the flavor dependence on the quark GPDs in the same manner with the unpolarized PDF determination.

We also note that there were related works recently on the electroweak process  $\ell N \rightarrow \nu \pi N'$  to investigate the GPDs at the future EICs [56]. Our current studies could be extended to such processes.

#### ACKNOWLEDGMENTS

The work was partially supported by Strategic Priority Research Program of the NSFC under Grant No. 12293060 and No.12293061, Chinese Academy of Sciences under Grant No. XDB34030301, and the CAS president's international fellowship initiative under Grant No. 2022VMA0003. It was also partially supported by the Japan Society for the Promotion of Science (JSPS) Grants-in-Aid for Scientific Research (KAKENHI) Grant Number 19K03830. The authors would like to thank B.

Pire, L. Szymanowski, and J. Wagner for suggestions on pion-production cross sections, R. Petti for communica-

tions on the Fermilab neutrino GPD experiment, and Wen-Chen Chang, S. V. Goloskokov, and P. Kroll for suggestions on the GPD parametrization.

- 
- [1] For reviews, see M. Diehl, *Phys. Rep.* **388**, 41 (2003); X. Ji, *Annu. Rev. Nucl. Part. Sci.* **54**, 413 (2004). For recent works, see H. Moutarde, P. Sznajder, and J. Wagner, *Eur. Phys. J. C* **78**, 890 (2018); Y. Guo *et al.*, *JHEP* **05**, 150 (2023).
- [2] B. Berthou *et al.*, *Eur. Phys. J. C* **78**, 478 (2018); PARTONS project, <http://partons.cea.fr/partons/doc/html>.
- [3] For reviews and recent works, see, for example, X. Ji, *Front. Phys.* **16**, 64601 (2021); C. Lorcé, *Eur. Phys. J. C* **78**, 120 (2018); C. Lorcé, A. Metz, B. Pasquini, and S. Rodini, *JHEP* **11**, 121 (2021).
- [4] M. Masuda *et al.* (Belle Collaboration), *Phys. Rev. D* **93**, 032003 (2016).
- [5] S. Kumano, Qin-Tao Song, and O. V. Teryaev, *Phys. Rev. D* **97**, 014020 (2018). See also prior works in M. Diehl, T. Gousset, B. Pire, and O. Teryaev, *Phys. Rev. Lett.* **81**, 1782 (1998); M. Diehl, T. Gousset, and B. Pire, *Phys. Rev. D* **62**, 073014 (2000).
- [6] Y. P. Xie and V. P. Goncalves, *Phys. Lett. B* **839**, 137762 (2023); *Eur. Phys. J. C* **83**, 528 (2023)
- [7] Y. Hatta and D.-L. Yang, *Phys. Rev. D* **98**, 074003 (2018); Y. Hatta, A. Rajan, and D.-L. Yang, *Phys. Rev. D* **100**, 014032 (2019); Rong Wang, Wei Kou, Ya-Ping Xie, and Xurong Chen, *Phys. Rev. D* **103**, L091501 (2021).
- [8] Y. Hatta, A. Rajana, and K. Tanaka, *JHEP* **12**, 008 (2018); K. Tanaka, *JHEP* **01**, 120 (2019); T. Ahmed, L. Chen, and M. Czakon, *JHEP* **01**, 077 (2023).
- [9] V. D. Burkert, L. Elouadrhiri, and F. X. Girod, *Nature* **557**, 396 (2018); For reviews, see M. V. Polyakov and P. Schweitzer, *Int. J. Mod. Phys. A* **33**, 1830025 (2018); V. D. Burkert, L. Elouadrhiri, F. X. Girod, C. Lorce, P. Schweitzer, and P. E. Shanahan, *Rev. Mod. Phys.* **95**, 041002 (2023).
- [10] H. Kawamura and S. Kumano, *Phys. Rev. D* **89**, 054007 (2014); H. Kawamura, S. Kumano, T. Sekihara, *Phys. Rev. D* **88**, 034010 (2013); W.-C. Chang, S. Kumano, and T. Sekihara, *Phys. Rev. D* **93**, 034006 (2016).
- [11] E. R. Berger, M. Diehl, and B. Pire, *Phys. Lett. B* **523**, 265 (2001); S. V. Goloskokov and P. Kroll, *Phys. Lett. B* **748**, 323 (2015); T. Sawada *et al.*, *Phys. Rev. D* **93**, 114034 (2016).
- [12] S. Kumano, M. Strikman, and K. Sudoh, *Phys. Rev. D* **80**, 074003 (2009).
- [13] For the recent situation, see the talk slides of Wen-Chen Chang at <https://indico.ectstar.eu/event/176/timetable/#all.detailed>; S. Sawada and N. Tomida at <https://kds.kek.jp/event/49330/>, <https://indico.phy.anl.gov/event/49/>.
- [14] S. Diehl *et al.*, arXiv:2405.15386.
- [15] R. Boussarie, B. Pire, L. Szymanowski, and S. Wallon, *JHEP* **02**, 054 (2017); Erratum, *JHEP* **10**, 029 (2018); A. Pedrak, B. Pire, L. Szymanowski, and J. Wagner, *Phys. Rev. D* **101**, 114027 (2020); O. Grocholski, B. Pire, P. Sznajder, L. Szymanowski, and J. Wagner, *Phys. Rev. D* **104**, 114006 (2021); **105**, 094025 (2022); J-W. Qiu and Z. Yu, *JHEP* **08**, 103 (2022); *Phys. Rev. D* **107**, 014007 (2023).
- [16] S. V. Goloskokov, Y. P. Xie and X. Chen, *Commun. Theor. Phys.* **75**, 065201 (2023); *Chin. Phys. C* **46**, 123101 (2022)
- [17] E. R. Berger, F. Cano, M. Diehl, and B. Pire, *Phys. Rev. Lett.* **87**, 142302 (2001); Bao-Dong Sun and Yu-Bing Dong, *Phys. Rev. D* **96**, 036019 (2017); W. Cosyn and B. Pire, *Phys. Rev. D* **98**, 074020 (2018).
- [18] Dongyan Fu, Bao-Dong Sun, and Yubing Dong *Phys. Rev. D* **105**, 096002 (2022); **106**, 116012 (2022); **107**, 116021 (2023); Dongyan Fu, Yubing Dong, and S. Kumano, *Phys. Rev. D* **109**, 096006 (2024).
- [19] J. Rout *et al.*, *Phys. Rev. D* **102**, 116018 (2020).
- [20] S. Kumano and R. Petti, PoS (NuFact2021) 092 (2022).
- [21] D. Adey *et al.*, arXiv:1308.6822 [physics.acc-ph] C. C. Ahcida *et al.*, CERN-PBC-REPORT-2019-003 (2020).
- [22] Xianguo Lu, personal communications (2024).
- [23] B. Lehmann-Dronke and A. Schafer, *Phys. Lett. B* **521**, 55 (2001).
- [24] P. Amore, C. Coriano, and M. Guzzi, *JHEP.* **02**, 038 (2005).
- [25] C. Coriano and M. Guzzi, *Phys. Rev. D* **71**, 053002 (2005).
- [26] A. Psaker, W. Melnitchouk, and A. V. Radyushkin, *Phys. Rev. D* **75**, 054001 (2007).
- [27] G. R. Goldstein, O. G. Hernandez, S. Liuti, and T. McAskill, *AIP Conf. Proc.* **1222**, 248 (2010).
- [28] B. Z. Kopeliovich, I. Schmidt, and M. Siddikov, *Phys. Rev. D* **86**, 113018 (2012).
- [29] B. Z. Kopeliovich, I. Schmidt, and M. Siddikov, *Phys. Rev. D* **89**, 053001 (2014).
- [30] B. Pire and L. Szymanowski, *Phys. Rev. Lett.* **115**, 092001 (2015).
- [31] M. Siddikov and I. Schmidt, *Phys. Rev. D* **95**, 013004 (2017).
- [32] B. Pire, L. Szymanowski, and J. Wagner, *Phys. Rev. D* **95**, 094001 (2017).
- [33] B. Pire, L. Szymanowski, and J. Wagner, *Phys. Rev. D* **95**, 114029 (2017).
- [34] R. Kunitomo, Bachelor's thesis, Japan Women's University (2023).
- [35] S. J. Brodsky and G. P. Lepage, pp. 93-240 in *Perturbative quantum chromodynamics*, edited by A. H. Mueller (World Scientific, 1989).
- [36] V. L. Chernyak and A. R. Zhitnitsky, *Phys. Rept.* **112**, 173 (1984).
- [37] G. P. Lepage and S. J. Brodsky, *Phys. Lett. B* **87**, 359 (1979); A. V. Efremov and A.V. Radyushkin, *Phys. Lett. B* **94**, 245 (1980).
- [38] P. Kroll, H. Moutarde, and F. Sabatié, *Eur. Phys. J. C* **73**, 2278 (2013).
- [39] V. M. Braun *et al.*, *JHEP* **04**, 082 (2017); M. V. Polyakov and Hyeon-Dong Son, *Phys. Rev. D* **102**, 114005 (2020).
- [40] K. Goeke, M. V. Polyakov, and M. Vanderhaeghen, *Prog.*



- Part. Nucl. Phys. **47**, 401 (2001).
- [41] M. Penttinen, M. V. Polyakov, and K. Goeke, Phys. Rev. D **62**, 014024 (2000).
- [42] R. P. Feynman, p.91 in *Photon-Hadron Interactions* (W. A. Benjamin, Inc., 1972).
- [43] Sec. 8.5 of F. Halzen and A. D. Martin, *Quarks and Leptons: An Introductory Course in Modern Particle Physics* (John Wiley & Sons, 1984).
- [44] V. Bertone, H. Dutrieux, C. Mezrag, H. Moutarde, and P. Sznajder Phys. Rev. D **103**, 114019 (2021); E. Moffat, A. Freese, I. Cloet, T. Donohoe, L. Gamberg, W. Melnitchouk, A. Metz, A. Prokudin, and N. Sato, Phys. Rev. D **108**, 036027 (2023).
- [45] M. Guidal, M. V. Polyakov, A. V. Radyushkin, and M. Vanderhaeghen, Phys. Rev. D **72**, 054013 (2005).
- [46] S. V. Goloskokov and P. Kroll, Eur. Phys. J. C **50**, 829 (2007); C **53**, 367 (2008); C **59**, 809 (2009); A **47**, 112 (2011).
- [47] S. V. Goloskokov and P. Kroll, Eur. Phys. J. C **65**, 137 (2010); A **47**, 112 (2011); A **50**, 146 (2014).
- [48] M. Vanderhaeghen, P. A. M. Guichon, and M. Guidal, Phys. Rev. D **60**, 094017 (1999).
- [49] S. V. Goloskokov, personal communications (2024); I. Larin *et al.*, Phys. Rev. Lett. **106**, 162303 (2011).
- [50] S. Kumano, Phys. Rep. **303**, 183 (1998); G. Garvey and J. C. Peng, Prog. Part. Nucl. Phys. **47**, 203 (2001); J. C. Peng and J. W. Qiu, Prog. Part. Nucl. Phys. **76**, 43 (2014).
- [51] M. Diehl, Th. Feldmann, R. Jakob, and P. Kroll, Eur. Phys. J. C **39**, 1 (2005).
- [52] M. Diehl and W. Kugler, Eur. Phys. J. C **52**, 933 (2007).
- [53] P. Kroll, Mod. Phys. Lett. A **35**, 2050093 (2020).
- [54] T. Cal *et al.* (MINER $\nu$ A Collaboration), Nature **614**, 48 (2023).
- [55] S. Ahmad, G. R. Goldstein, and S. Liuti, Phys. Rev. D **79**, 054014 (2009).
- [56] M. Siddikov and I. Schmidt, Phys. Rev. D **99**, 116005 (2019); B. Pire, L. Szymanowski, and J. Wagner, Phys. Rev. D **104**, 094002 (2021).